Efficiency meets Sky

Joint NASA / DLR Aeronautics Design Challenge 2017-2018

Institute for Aeronautics and Astronautics
Department of Aircraft Design and Aerostructures
Prof. Dr.-Ing. A. Bardenhagen

Technische Universität Berlin

TU Berlin | ILR Sekr. F2 | Marchstraße 12-14 | 10587 Berlin

German Aerospace Center (DLR)
Institute of System Architectures in Aeronautics
Aircraft Design & System Integration
c/o ZAL TechCenter
Hein-Saß-Weg 22
D-21129 Hamburg
z.H. Dr.-Ing. Johannes Hartmann

Fakultät V Verkehrs- und Maschinensysteme
Institut für Luft- und Raumfahrt

FG Luftfahrzeugbau und Leichtbau

Fachgebietsleiter
Prof. Dr.-Ing.
Andreas Bardenhagen

Sekretariat F2 Raum F 126
Marchstraße 12-14
10587 Berlin

Telefon +49 (0)30 314-28538
Telefax +49 (0)30 314-22955
Andreas.Bardenhagen@tu-berlin.de

Team Assistenz im Sekr. F2
M.A. Anke Heymann

Telefon +49 (0)30 314-22954
Telefax +49 (0)30 314-22955
Anke.Heymann@tu-berlin.de

Unser Zeichen:
F2 Bh/He

Berlin, 28.06.018

Joint NASA / DLR Aeronautics Design Challenge // Selbstständigkeitserklärung

Sehr geehrter Herr Hartmann,

hiermit bestätige ich, dass die angefertigte Arbeit mit dem Thema:

„Efficiency meets Sky“

selbstständig sowie ohne unerlaubte fremde Hilfe und ausschließlich unter Verwendung der aufgeführten Quellen von den Studierenden

- Beck, Ramon
- Bieler, Juri
- Borsutzki, Simon
- Cabac, Yannic
- Dehmel, Jiri
- Khosravi, Raman
- Klünder, Arthur
- Kracke, Lennart
- Lopez Milan, Jorge
- Roscher, Stephanie
- Rüthnik, Pascal

angefertigt wurde.

Mit freundlichen Grüßen

TECHNISCHE UNIVERSITÄT BERLIN
Institut für Luft- und Raumfahrt
FG Luftfahrzeugbau und Leichtbau
Sekr. F2
Marchstraße 12-14 • D-10587 Berlin

Andreas Bardenhagen

> Seite 1/1

Table of Contents

List of Figures

List of Tables

Nomenclature

Indizes

Symbol	Designation
aft	After Center Body
CL	Climb
CR	Cruise
D	Drag
equi	Total Resistant
f	Fibre
fuse	Fuselage
g	Gravity Force
gas	Gaseous
H2	Hydrogen
ICA	Initial Cruise Altitude
in	Internal
K	Kerosene
L	Lift
LD	Landing
MTOM	Maximum Take Off Mass
neo	New Engine Option
R	Range
to	Take Off
w	Wetted

Abbreviations

Abbreviation	Designation
ACAP	Aircraft Characteristics for Airport and Maintenance Planning
ADHF	Adaptive Dropped Hinge Flap
ATM	Air Traffic Management
BLI	Boundary Layer Ingestion
BPR	Bypass Ratio
BWB	Blended Wing Body
BYOD	Bring Your Own Device
CAD	Computer Aided Design
CFD	Computational Fluid Dynamics
CS	Certification Specifications
DOC	Direct Operating Costs
EFB	Engine Feature Benefit
EIS	Entry Into Service
ER	Extended Range
FOD	Foreign Object Damage
FFF	Fuel Fraction Factors
FRB	Fuel Reduction Benefits
FST	Full-Size-Trolley
GDP	Gross Domestic Product
GE	General Electric
GTF	Geared Turbofan
GVPTF	Geared Variable Pitch Turbofan
GWP	Global Warming Potential
HST	Half-Size-Trolley
ICA	Initial Cruise Altitude
ICAO	International Civil Aviation Organization
IFFF	Improved Fuel Fraction Factors
IRA	Intercooled Recuperated Aero Engine
ISA	ICAO Standard Atmosphere
LR	Long Range
LTO	Landing and Take Off Cycle
MLI	Multi Layer Insulation
NO	Nitrogen Oxides
PAX	Passengers
pkm	passenger kilometer
PW	Pratt & Whitney
RFFF	Roskam Fuel Fraction Factors

RFI	Radiative Forcing Index
RPK	Revenue Passenger Kilometer
SET	Specific Excess Thrust
SFC	Specific Fuel Consumption
SMK	Seat Mile Kilometers
SRIA	Strategic Research and Innovation Agenda
STE	Specific Transport Energy
SU	Standard Unit
TFFF	Taxi Fuel Fraction Factor
TOFL	Take Off Field Length
TRL	Technological Readiness Level
UHC	Unburned Hydrocarbons
VLA	Very Large Aircraft
VPF	Variable Pitch Fan

Challengers

BECK,
RAMÓN
Expertise:
Tank Design

BIELER,
JURI
Expertise:
Airfoil Optimization

BORSUTZKI,
SIMON
Expertise:
CAD

CABAC,
YANNIC
Expertise:
Centerbody Design

DEHMEL,
JIRI
Expertise:
Propulsion System

KHOSRAVI,
RAMAN
Expertise:
Cabin

KLÜNDER,
ARTHUR
Expertise:
CAD

KRACKE,
LENNART
Expertise:
Aerodynamics

LOPEZ MILAN,
JORGE
Expertise:
Tank Design

ROSCHER,
STEPHANIE
Expertise:
Cabin

RÜTHNICK,
PASCAL
Expertise:
Reference A/C

1 The Need for Change

"Beim Erdöl liegt die Zukunft hinter uns." (Josef Auer, Analyst) [1]

Before the existence of modern civilization, the atmospheric concentration of CO_2 remained generally constant. Since then the average concentration of carbon dioxide suddenly increased up to 2013 when it surpassed a level of 400 ppm for the first time in recorded history [2]. This manifests itself in an emission of more than 1,100 tonnes of carbon dioxide per second, equal to 35.76 gigatonnes per year (status as of 2016) [3], while only one half is recycled back into the carbon cycle [4]. Although the share of global anthropogenic CO_2 emitted by the aviation industry is only 2% [5], it plays an important role in fighting the climate change due to its high radiative forcing index (RFI). This factor takes into account that aside from CO_2 air traffic also emits numerous other climate-relevant emissions, like NOx, soot, and contrails into the atmosphere whose warming effects are significantly larger due to output in particularly sensitive, high altitude atmospheric layers. This results in a two to four times greater climate impact of aircraft compared to CO_2 emissions alone and underlines the indispensability of using RFI as a benchmark. Therefore, the aviation sector, as the only artificial emission source at high altitude, has a climate and environmental responsibility to develop sustainable air transportation with almost negligible CO_2 input. Although airlines have reduced their fuel consumption in recent years and transport capacity is increasingly decoupled from fuel consumption [6], absolute CO_2 emissions have increased as a result of the simultaneously rising traffic volume. With an average annual growth of 5% and a doubling of air traffic every 15 years [7], this is insufficient to achieve aviation's high-level emission reduction goals defined by NASA and the European Commission in Flightpath 2050 [8] which have been developed to reconcile the future needs of aviation with environmental objectives such as the Paris Agreement [9]. It is the responsibility of mankind to proactively adapt to changing conditions in order to ensure not only environmentally sustainable technology, but also improved operations, efficient infrastructure and adapted economic measures [10]. The component wise improvement of a classic "tube and wing" aircraft configuration may not be able to deliver the required enhancements at aircraft level. Consequently, key to meeting ambitious future demands are disruptive configurations and synergistically integrated systems paving the inevitable process of transition.

The purpose of this design study is to present a valid preliminary next level aircraft concept with entry into service (EIS) in 2045 using a wide range of promising technologies and leading in a new fuel era. Innovative aircraft operations, the passenger acceptance and possible modifications in the airport infrastructure have to be taken into consideration.

To develop a sustainable and successful concept it is mandatory to discover the future markets needs. Therefore the following layout is based on both a market analysis and a technology outlook, taking the availability of technologies, expressed through the Technological Readiness Level (TRL) into account. Due to the analysis the top level requirements of the present aircraft design were defined aiming further detailing in the progressive design process to develop suitable solutions. Based on these considerations the reference aircraft is selected. With the help of relevant literature and established calculation methods, several configurations have been elaborated, however, only the final results refined in several iterations are presented. To validate the integration into the overall air traffic system, the concept is subjected to a feasibility study in order to identify solution approaches to possible challenges. Assessing the competitiveness of the design and the achievement of the set goals, the sustainability of the concept is finally evaluated from different perspectives.

It should be noted that this is a preliminary draft to point out future solutions, which forms the basis for more detailed concept studies.

2 The Aircraft of Tomorrow

Along with the proposed goals set by various organizations the focus of commercial aircraft design is increasingly shifting from minimizing operation costs to environmental compatibility, creating an impetus for high-efficient low emission aircraft design. To subsequently select a suitable reference aircraft for EIS 2045 the future market has to be addressed.

2.1 Potential of Future Markets

The following market analysis makes it possible to detect global trends about the future development of aviation and to derive possible scenario forecasts. As the aviation segment is a resilient and steadily growing market, there will be a major need for new aircraft in the future, with single-aisle aircraft representing 70% of the demand in units, whereas long-haul aircraft account for 55% of value [7]. Demand cannot be assumed as constant but varies by region. While the growth of established markets like Northern America or Europe is increasingly stagnating, the emerging markets, e.g. the Asia-Pacific region, are characterized by very high growth rates due to the strong correlation between revenue passenger kilometre (RPK) and gross domestic product (GDP) [11]. The demand of very large aircraft (VLA) such as the Boeing 747 or the Airbus A380 is powered by aviation mega-cities, which are driving global air traffic growth and handling 95% of all long-haul flights in the future [12]. As already mentioned, airlines have reduced their fuel consumption in recent years. Albeit long-haul traffic has a specific fuel consumption of just 3.51l/100pkm (medium-haul: 3.98l/100pkm, short-haul: 5.86l/100pkm), with 60% it makes a comparatively large contribution to total fuel usage [13]. Caused by the large flight distance and the high number of passengers this results in greater absolute CO_2 emissions with an increased climatic effect due to high altitudes. The combination of all stated constraints suggests the long-haul market to be very promising.
In order to ensure sustained growth in passenger demand, a flexible and expanding network is required [14]. For being able to assess the behavior of this network, it is essential to consider the various factors that influence its framework conditions, like political and legal basics and fuel availability. Based on this two main scenarios are conceivable which result in the abandonment of fossil fuels: Firstly, the taxation of pollutant emissions due to political environmental protection requirements makes the use of conventional fuels unprofitable. Secondly, fossil fuels are limited, which will inevitably lead to the depletion of those resources. As a consequence the ultimate solution approach would be a non-polluting fuel produced from renewable sources. Several fuel concepts were discussed and finally an overall design concept tailored to the use of hydrogen was sought, considering it as the most promising.
In addition to low emissions hydrogen offers the great advantage of a three times higher energy density compared to kerosene but due to the very low volumetric energy density (hydrogen has only about 1/4 of the volumetric energy density of kerosene) it requires the necessary provision of additional volume to accommodate the fuel [15]. Consequently there are some challenges, which have to be addressed, in order to establish a sustainable, efficient and competitive configuration. Bearing this in mind using a hydrogen-powered blended-wing-body configuration serving long-haul routes, the design process is driven towards meeting the market requirements while maximizing the synergy effects issued by the hydrogen concept.

2.2 Reference Aircraft

In order to assess the designed aircraft with regard to the requirements to be met, it is necessary to first select a reference aircraft. This defines the specific mission requirements, especially in terms of range and payload, as well as the take off and landing performance that are to be achieved. Compared with this aircraft, an energy reduction of at least 60%, 80% in the long term, as well as a noise reduction of 42-52dB and a NOx reduction of at least 80% has to be attained.
To select the most suitable Best-in-Class aircraft a basic approach has been developed to assess several aircraft using standardized criteria and comparison parameters. In a first step the classes itself and the corresponding class criteria are set up, elaborating the range and size of the airplanes

as important system descriptors. Accordingly the following classes are distinguished: Narrow-body aircraft and wide-body aircraft, which can additionally be divided up into single- and double-deck wide-body aircraft. As it is not possible to compare the aircraft by taking the fuel consumption per mile into account, since every aircraft has a unique design point, another measure of efficiency has to be found. In order to determine which aircraft has the best energy efficiency in the different classes, the payload range diagram is used which indicates every possible combination of payload and range for a specific aircraft type and can be found in the respective ACAP (Aircraft Characteristics for Airport and Maintenance Planning). Therefore one characteristic point is identified in which the various aircraft are comparable, namely the point of maximum range at maximum payload (hereinafter referred to as "Point B")(see Appendix A.1). Given the fuel and payload mass, as well as the range in Point B, the specific transport energy (STE) can be defined as a comparison parameter.

$$STE = \frac{g \cdot m_{Payload,MTOM} \cdot R}{m_{Fuel,MTOM}} \tag{2.1}$$

Since the STE represents the ratio of conducted work to burnt fuel, a high STE indicates the best-in-class aircraft. Table 2.1 shows the results of relevant comparison aircraft. Single-aisle aircraft are not considered due to the previous findings of the market analysis.

Table 2.1: Specific transport energy of relevant aircraft

Class	Aircraft	Payload [kg]	Fuel [kg]	Range [NM]	STE [$\frac{J}{kg}$]
wide-body, single-deck	Airbus A340-300	52,685	98,500	5,653	54,929,275
	Boeing 777-200ER	56,940	91,900	5,180	40,960,960
	Airbus A330-200	49,442	63,000	4,169	59,441,579
	Boeing 777-300ER	69,853	113,852	5,660	63,091,495
	Boeing 777-200LR	63,957	138,346	7,586	63,712,948
wide-body, double-deck	Boeing 747-400	67,319	150,820	5,180	42,006,691
	Airbus A380	83,800	206,000	5,180	48,458,106
	Boeing 747-400ER	70,307	161,025	6,333	48,864,781

Due to the anticipated strong growth and the fact that the BWB configuration can exploit its advantages especially in the VLA segment [16] the reference aircraft is selected from the wide-body double-deck class. Consequently the Boeing 747-400ER with PW4062 engines is chosen as the reference aircraft, resulting in the mission and performance requirements shown in Table 2.2.

Table 2.2: B747-400ER design data [17]

Reference aircraft data	
Number of PAX (all economy seating)	524
Design point range [NM]	6,160
Design point fuel [kg]	161,025
Initial cruise height [m]	1,0363
Takeoff field length [m]	3,095
Landing field length [m]	2,164
Aproach Velocity [kts]	153

As seen in Appendix C.1 various key technologies have been identified to target the top level requirements. To ensure feasibility a TRL of at least 5 is assumed. In the following section the overall configuration is presented which is based on the optimal exploitation of synergy effects to meet future goals.

3 Ultra-efficient Design

Due to the decreasing scale of improvement of nowadays common aircraft configurations and components, a radically new concept is needed to fulfill the demands and challenges of emerging future air traffic, its emissions and impacts towards mankind and environment. Therefore, this concept is driven by a most sustainable propulsion and fuel concept and then designed around those two aspects with consideration of typical aircraft design parameters such as a high lift-to-drag ratio, low noise emissions, fuel efficiency and passenger comfort [8], [18]. The following sections offer an overview of used technology and their implementation into the concept design.

3.1 Blended-Wing Configuration

Common aircraft configurations suffer from stagnation in improvement as well as from an above all sub-optimal distribution of weight alongside their components. Typically the payload is located in the fuselage, causing the major weight towards ground. Meanwhile, most if not all of the lift is generated by the wing with a relatively huge distance between its respective point of attack and the fuselage's. This leads to huge amounts of bending stress on the connecting parts between wing and fuselage, which forces structure to be enhanced in these areas.
Aiming towards a reduction of these effects, a blended-wing-body (BWB) configuration is introduced bringing more than one positive side effect. First, due to a steady transition from body to wing and thus no bottlenecks in flux flow, the structural stress is significantly lower compared to a conventional configuration. Second, the pure geometry offers a much bigger area to generate lift, resulting in much lower wing loads. This considers the center body creating lift as well and hereby putting the above mentioned relative points of attack closer together. Third, expecting the air flow following the contour of the airfoil especially over the center body, putting the engines aft provides boundary layer ingestion improving the effectiveness even more. Additionally, the aft positioning causes a small distance between engine and center-axis spanwise, so in case of engine failure, just a small yaw momentum would be generated. Last but not least, putting the engines on the top of the aircraft, noise emission is directed upwards, reducing the noise on lower flight levels and during take off and landings. In addition, this also reduces the necessary distance between ground and aircraft because there is no clearance angle to be met in case of front wheel breakdown in order to prevent the engines from touching the surface.
As already stated, the BWB offers a bigger surface area than conventional configurations, resulting in a greater enclosed volume. To fully exploit that characteristic, every geometry is distributed to that, e.g. the tanks and cabin tubes are perfectly fitted into the shape by self-written algorithms (described below).
All in all, a BWB with V-tail, embedded aft engines, advanced surface control faces, no APU and a multi-boogie gear arrangement is selected. Lastly mentioned are explained later on. The final configuration is presented below (figure 3.1 and figures Appendix L.1 to Appendix L.3.

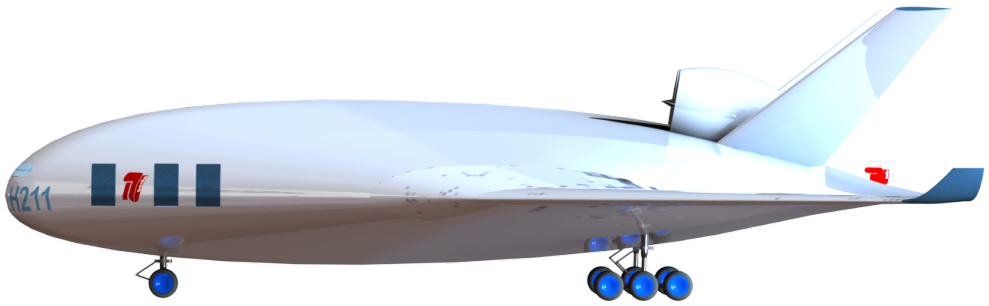

Figure 3.1: Sideview rendered

3.1.1 Multi-Bubble Centerbody Design

The first step in this BWB design method is the selection of airfoils for the centerbody. Compared to the airfoil selection for common tube-wing-configurations, there are only a few freely accessible airfoils for BWBs or flying wings, especially outside of model aircraft applications. For passenger aircraft, the centerbody has to contain the cabin tubes which in turn necessitates a high airfoil thickness ratio. Meanwhile, the centerbody has to generate the necessary lift while minimizing the resulting drag. Therefore, a careful aerodynamic and geometric optimization is required.

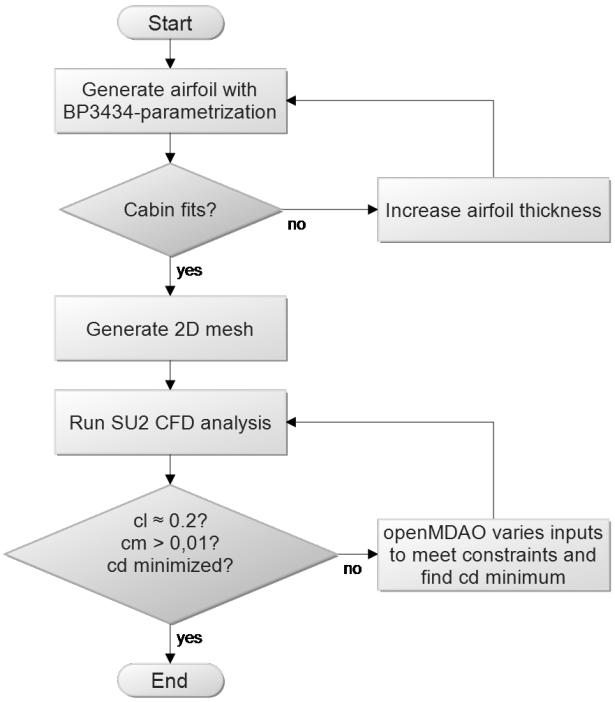

Figure 3.2: Airfoil optimization flowchart

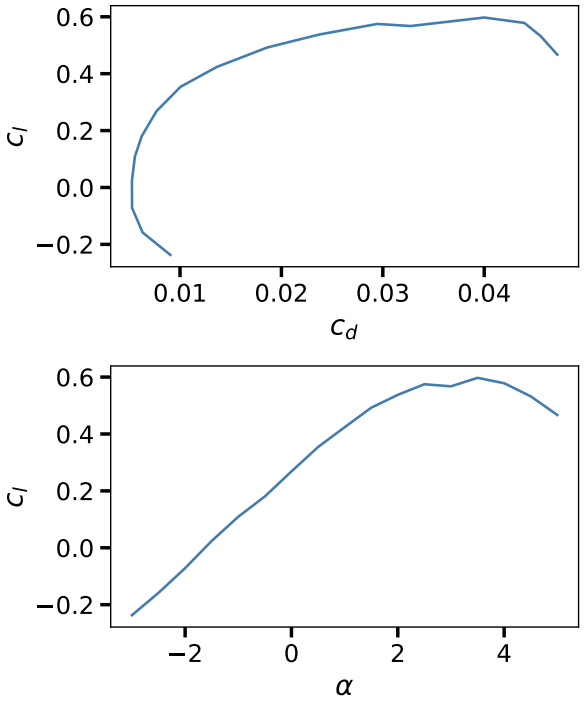

Figure 3.3: Polar of the center-body-airfoil

To simplify this task the three dimensional problem is reduced to a single two dimensional airfoil. To describe the shape of the airfoil to be optimized, a Bézier-Parsec-3434 (BP3434) parametrization as described by Derksen and Rogalsky [19] is used. Camber and thickness of the airfoil are derived from two bezier curves each, split at the point of maximum camber/thickness. The leading edge curves are third degree bezier curves and the trailing edge curves are fourth degree bezier curves to allow an exact shaping of the trailing edge to meet the moment requirements of a BWB. This amounts to 18 control points in total resulting in 28 variables considering the set starting point and the set connection between leading edge and trailing edge curve. The advantage of the BP3434 parametrization is the calculation of these variables using 10 aerodynamic parameters such as leading edge radius or trailing edge angle plus four additional bezier parameters. This leads to faster fitting to the starting airfoil and faster convergence of the whole aerodynamic optimization [19].
The next step is the thickening of the airfoil to integrate the cabin, represented by a rectangle. The desired utilization factor of the airfoil can be set by setting the length of the sides of the rectangle. Now a 2D C-Mesh is generated around the airfoil and its aerodynamic properties are analyzed in a CFD simulation with SU2 using Navier-Stokes-algorithm. Using the optimization platform openMDAO created by NASA, the parameters are varied with the objective to minimize drag while still satisfying the lift and moment coefficient constraints. This process is shown in figure 3.2. After this time-consuming optimization converges, further analysis with different angle of attack is done with the found airfoil, to generate the polar shown in figure 3.3. Figure 3.4 shows the optimized airfoil with the cabin as well as the starting airfoil, which could not contain the cabin. Due to the huge amount of computational power needed and the limited time, the chosen airfoil does not represent the best possible solution yet, but the optimization process proved to be working and

can be used for future projects. The airfoil optimization is handled two-dimensional but for an

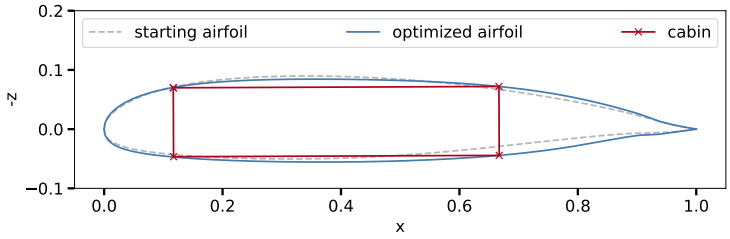

Figure 3.4: Optimized airfoil

optimized shape, a 3D consideration of the geometry has to be considered. Therefore, an algorithm is created, that is looking for intersection points between the radial outer tube surface and the inner shape surface to prevent the tube from "sticking" out.

3.1.2 Wing Design

The main difference in designing a wing for a blended-wing configuration is the need to adjust to a given centerbody planform with predetermined airfoil and very small margins for twist. The challenge is to satisfy the requirements for stability and provide the necessary lift while minimizing the drag of the aircraft in cruise condition by making minor adjustments to the wing planform and twist distribution. This is achieved by an iterative design process characterized by rising fidelity.
The first step is the definition of a wing loading using the methods described in section 4.3.1. The resulting wing area is calculated by using the first mass estimation and the given geometry of the centerbody. The wing planform is determined by adding further geometric constraints like wing span, aspect ratio, taper ratio and leading edge sweep. The wing span is properly dimensioned, when the lever-arm fulfills the requirements for controllability. Besides, a high wing span, and therefore a high aspect ratio, is advantageous due to the minimization of induced drag. However, a wing span of 80 metres must not be exceeded with respect to the existing airport infrastructure. The airfoil MH49 is selected for the wing due to its low moment coefficient and camber [20]. Further improvements of the aerodynamic design are possible by using the airfoil optimizer described in the previous section to generate the optimal airfoil for each individual spanwise position.

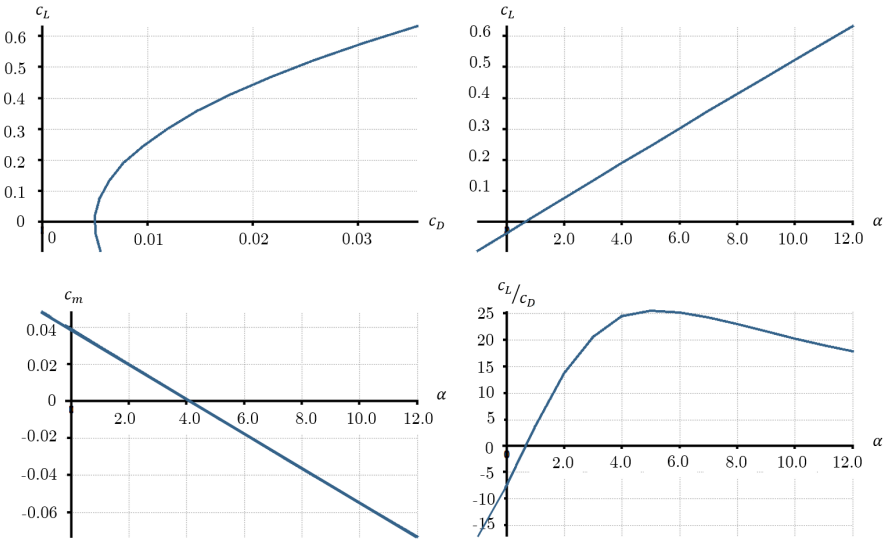

Figure 3.5: BWB polars calculated in XFLR5

The next step is the analysis of the aircraft with the software XFLR5 using a low fidelity vortex lattice method. Planform and twist modifications are applied to satisfy stability requirements and to accomplish an elliptical lift distribution to reduce induced drag. In order to achieve a stationary,

stable and trimmed flight condition the following two requirements need to be matched. First the pitching moment must equal zero. Second the centre of gravity is positioned in front of the aerodynamic centre which is equivalent to a negative gradient of the moment coefficient polar. Consequently, the moment coefficient at zero lift must be greater than zero [21]. The center of gravity, as an outcome of the mass breakdown, is estimated to 19.7m measured from the nose of the center body. The resulting moment coefficient polar, which is illustrated in figure 3.5, shows that both requirements for static stability are fulfilled. In the course of the conceptual design further flight mechanical aspects, such as controllability, will not be elaborated on. Nevertheless, simple design methods already lead to primary control surfaces as shown in chapter 3.1.3. The resulting polar plots are shown in figure 3.5. The resulting geometric parameters of the whole BWB aircraft are shown in table 3.3. The last step is the analysis of the aircraft with a full CFD simulation in

Table 3.3: Aircraft geometric parameters

Parameter	Unit	Value
Wing area	[m^3]	1317
Aspect Ratio	[-]	4.62
Wing Span	[m]	79.5

openFOAM using the rhoSimpleFoam solver for turbulent flow of compressible fluids [22] with a k-ω-SST turbulence model to verify the results of the previous analysis. The pressure distribution and streamlines at cruise condition are shown in figure 3.6. The CFD analysis shows that the requirements to the pitching moment aren't satisfied yet. Also, the drag coefficient is too high due to the strong shocks in the transition from centerbody to wing caused by the non-optimized wing airfoil. Additional adjustments have to be made to reach the design objectives and to increase lift-to-drag ratio but would exceed the scope of this design study.

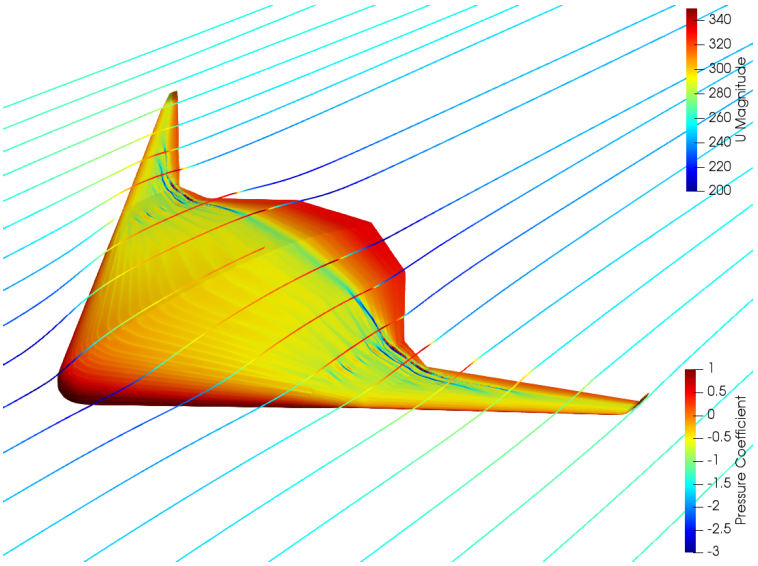

Figure 3.6: Pressure distribution and streamlines at cruise conditions

3.1.3 Multi Functional Control Surfaces

The common philosophy regarding surfaces tends to be a distribution with each surface executing one task (roll, pitch, yaw, deceleration). Trending towards multi-functional surfaces, technology will advance and result in lighter flap and spoiler systems, adaptive shape technology and even morphing structures. While the "morphing wing" is not to be accomplished in the next years, there is yet a promising approach today the Airbus A350 is already equipped with: The Adaptive Dropped Hinge Flap (ADHF) system. It basically simplifies the flap mechanisms, defining one flap at the rear edge that can be deflected down- and even upwards. Therefore, the wing shape can be adapted

to various in-flight situations, concluding in optimized lift and pressure distributions. Even a shift towards the tip or root of the wing is possible leading to improved distributions for take-off (T/O) and landing (LDG) configurations. The potential of reducing drag, noise and emissions is immense, hence improvement to aerodynamic systems will be essential in future aircraft development [23].
As far as the "traditional" control surfaces are concerned, the V-tail embeds yaw and pitch ability while reducing noise on ground and during T/O and LDG. This compensates the slightly increased drag due to the higher wetted area. For calculation, preliminary empirical, dimensioning in relation to other existing BWB studies is used (with results included in table Appendix I.1 in the Appendix).

3.2 Propulsion System

"Historically engines have been designed around fuel. It´s time to design the fuel around the engine's needs." (Robert Biddle, Fuels Technology Manager, Pratt & Whitney)

The engine as the aircraft's only active emission source offers the greatest potential savings in the field of noise and pollution reduction. As a result SRIA demands more than half of the savings to be realized through improvements of the engine [24]. To achieve this, there are several potential points of attack. In addition to the general reduction of fuel, both the improvement of individual components by new technologies and the implementation of new fuels are auspicious [25]. Apart from ensuring the reliability and safety standards of state-of-the-art engines the integration of new concepts in existing and new aircraft configurations must be guaranteed [26]. Since the present aircraft concept is operated with hydrogen, initially an adaptation of conventional engines to the new fuel has to be considered.

3.2.1 Adaption to Hydrogen

To optimally utilize the advantage of hydrogen in the engine, an adaptation of the combustion chamber is necessary. The main design objective for the combustion chamber is to provide a high combustion efficiency while keeping the production of air pollutants to a minimum. Hydrogen as fuel avoids the emission of sulfur oxides, carbon oxides, unburned hydrocarbons (UHC) and soot. The only remaining pollutants are water and nitrogen oxides (NO_x). Even though non-optimized combustors increase NO_x production, an optimized combustor provides the opportunity to lower NO_x emissions. To achieve this objective the main parameters for NO_x production need to be identified. Research by Levebre [27] shows that the main parameters for decreasing NO_x production are reaction rate, mixture and residence time. Lowering the reaction rate by decreasing the temperature or pressure of combustion would result in a decrease of engine efficiency. Increasing the mixedness poses a risk of flashbacks for hydrogen. Lowering the residence time of the reactants by increasing the air speed in the combustor could result in flame out.
The micromix hydrogen combustor tested by Boerner et al. [28] uses the effect of jet in cross-flow.

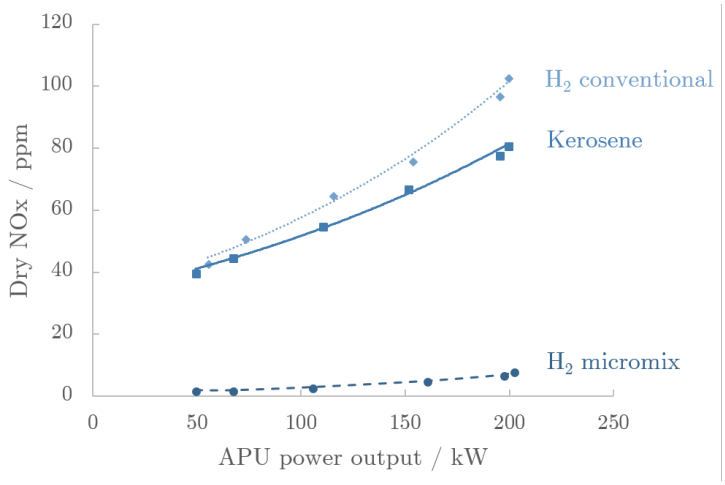

Figure 3.7: Test engine NO_x against power output [28]

By using the high reaction rate of hydrogen and injecting it vertically into the airstream from as many miniaturized injection holes as feasible, it burns in multiple small diffusion type flamelets instead of large flames. This results in optimal mixing and low residence time due to the short length of the flamelets which in turn results in much lower NO_x emissions than under kerosene operation as shown in figure 3.7.

3.2.2 Next Generation Technologies

Enhanced propulsive efficiency of a modern engine is significantly influenced by a high bypass ratio [29]. With increasing bypass ratio, the fan diameter grows [30] and leads to shock losses at the blade tips [29]. The geared turbofan enables the implementation of larger bypass ratios by decoupling fan and low-pressure turbine by a planetary gearbox providing fuel savings of up to 15 % compared to a conventional engine [31] and provides a reduction of perceived noise level by up to 50 % and lowers the noise foot print by 75 % [32]. The GTF with a set bypass ratio of 12 and an integrated hydrogen combustion chamber forms the basis of the next generation state-of-the-art jet engine. In order to meet the ambitious future demands it is necessary to implement additional high level improving technologies. The engine of a long-haul aircraft is designed for cruise flight [33]. Consequently, in all other flight phases it operates off-design due to deviating inflow conditions. A promising solution is an engine with variable fan blades, which actively influences the propulsion efficiency in the off-design by altering the blade pitch and thus specifically increases the engine's performance [34]. This allows further fuel saving potential of up to 13.5 % [35].

3.2.3 Engine to Aircraft

In addition to the component improvements, it is possible to achieve a further increase in efficiency through synergetic integration of the engine. For this reason, the two engines are embedded in the rear fuselage to take advantage of the promising concept of BLI. The growing boundary layer of the fuselage is sucked in and allows a reduction of total drag. This technology has the potential to reduce the aircraft fuel burn by another 8.5 % [36]. The current engine concept enables high fuel savings due to the optimized propulsion efficiency. Further savings are possible by increasing the thermal efficiency. This is made possible by the use of an IRA, which offers great potential for savings, so that the engine can be optimized with regard to overall efficiency. Since the mutual influence of these new technologies is difficult to estimate, the integration of the IRA concept is only considered for an H211neo variant. The advantages of the IRA concept are the increase in thermal efficiency [37] and the exploitation of the synergetic effects of hydrogen on the overall system [38]. The focus of the first approach is a safe, reliable and hydrogen-burning Geared Variable Pitch Turbofan (GVPTF). Technical data sheet of the GVPTF is listed in Appendix G.

3.3 Fuel System

In future aircraft scenarios, facing challenges to satisfy the global market growth requires new approaches in air transport solutions while simultaneously reducing the environmental impact. In this context, cryogenic fuels are reasonable candidates to reduce the overall energy consumption on a mission, and thus, the total aircraft footprint. Two candidates have great chances to become the replacement of Jet-A: liquid hydrogen (LH_2) and liquid methane (LCH_4). Both cryogenic fuels have a high specific energy, are lighter, thus reducing take-off mass and less polluting than Jet-A. However, more storage volume is needed, since both fuels possess less energy content per unit of volume. Table 3.4 compares the properties of the three mention fuels. As the reduction of energy

Table 3.4: Properties of Jet-A Fuel, LH_2 and LCH_4

Parameter	Unit	Jet-A Fuel	LH_2	LCH_4
Specific energy	[MJ/kg]	43.2	120	50
Specific density ρ	[kg/m^3]	790-808	71	423
Boiling point at 1 atm	[°C]	167-266	-252.3	-161
Freezing point at 1 atm	[°C]	-40	-259	-182

consumption and pollution are one of the major objectives, liquid hydrogen has been selected due to higher specific energy (roughly 2.8 higher energy per kilogram than Jet-A, and more than the double than LCH_4) and its lower well-to-wheel emissions in terms of greenhouse gases when comparing the three fuels. The combustion of liquid hydrogen produces water vapor whereas liquid methane produces harmful particles as CO, CO_2 and in a lower level, NO_x.

3.3.1 Tank Design

The design and development of the hydrogen tank as well as the design of an insulation, which could satisfactorily protect the tank from heat input, is one of the crucial technical challenges confronting the use of LH_2 [16]. Tank design and configuration are dependent on both aircraft (set an upper limit on the tank diameter) and engine configuration (amount of fuel to be stored). Cryogenic hydrogen exits in liquid phase only in a small range of temperature, since $-259°C$ and $-253°C$ are respectively freezing and boiling point [39]. Only 6°C keep the liquid hydrogen from evaporating, causing fuel loss (boil-off) due to pressure rise inside the tank. Therefore, insulation and tank wall material are truly important to respectively minimise boil-off and withstand the pressure rise due to vaporisation in severe temperature conditions. Moreover, hydrogen will be stored as a saturated liquid, at a combination of temperature and pressure where the vapor is saturated and in equilibrium with its liquid [38].

Tank Configuration At first sight, either integral or non-integral tanks should be chosen. Integral tanks are part of the fuselage while non-integral tanks are kept separate from the aircraft fuselage. Due to the non-cylindrical fuselage design, non-integral tank is concluded to be a better suitable option for the tank configuration. The advantages of this configuration is that the tank should only bear the loads associated with the fuel containment (pressurisation, fuel dynamic loads and thermal stresses). Regarding to the shape of the design the tank shape was optimized to minimize empty volume inside the center body. Three tanks are placed at each side in order to achieve the required volume. Each tank has different dimensions due to our center body design. The different measurements of the tanks are displayed in table 3.5. Another concern regarding the configuration is whether the insulation will be internal or external. As stated in [16], external insulation is selected because of the difficulty of meeting the requirement of impermeability to gaseous hydrogen if internal insulation would be used.

Another issue to address is the tank filling and venting pressure furthermore and its significant role. To allow venting a two-phase mixture needs to be present at all times. At least 3% of the volume should be in gas phase to allow venting when required [40]. Venting pressure of $p_{vent} = 1.5$ bar has been selected to minimize mass and maximize usable volume. In an emergency case due to rupture of thermal degradation of the insulation, the pressure will rise so rapidly that no fuel can be withdrawn. For safety reasons the fill level thus needs to be kept low enough to prohibit an excessive pressure rise in the tank if the vent valve would be blocked as well [38]. Filling pressure has been set to $p_{fill} = 1.2$ as it suggested by [38] in terms of safety aspects.

Tank Wall Material The choice of the material used for tank walls depends on its density, maximum allowable stress and, even more important, its behaviour when getting into contact with cryogenic hydrogen. As hydrogen molecules are very small, they tend to permeate through the tank wall material. When in contact with cryogenic hydrogen, embrittlement occurs for some materials, which can result in cracking at significant lower stress levels than yield strength [38]. Aluminum alloys are considered as tank wall material because they provide minimum susceptibility to embrittlement [41]. Although aluminum tanks are slightly heavier than composite tanks due to their higher density, their behaviour to cryogenic hydrogen in terms of embrittlement and permeation is superior compared to composites and already proven by previous investigations. Aluminum alloy 2219 is finally chosen as it fulfills the requirements for yield strength and embrittlement, besides it is also used by Air Liquide for the construction of the LH_2 tanks for the Ariane 4 launcher and thus proven to be suitable for this application.

Insulation Material The insulation system has to provide low thermal conductivity, low thermal diffusivity and low mass density. For this study three different insulation systems are considered:

multi layer insulation (MLI), aerogel and polymer foams. Especially in long range flights an appropriate insulation system is necessary to minimise losses due to boil-off. The figure in 7 displays the density respectively the thermal conductivity of various insulation materials. It shows that polymer foams offer the best solution as they offer a low thermal conductivity and a low density. Multi layer insulation with vacuum jackets can reach thermal conductivity two orders of magnitude lower than the best polymer foams [41]. However, a collapse of the vacuum system would diminish the insulation effectiveness and thus heat leakage would cause a pressure rise inside the tank leading to rapid boil-off [38]. Finally, low density flexible foam is used as insulation material.

3.3.2 Mechanical design

Despite non-integral configuration, the tank has only been design to resist pressure loads. External loads and connections of the tank to structure are not feasible within the scope of this project. To compensate this simplification, a safety factor was considered. As mention in [38], the optimum venting pressure for a specific mission and aircraft size is a compromise between tank weight and the amount of fuel to vented or insulation weight. Since the material of the tank and the venting pressure have been selected in section 3.3.1, the thickness for cylindrical and spherical walls is calculated based on the ASME Boiler and Pressure vessel code [42]. Both thicknesses are calculated for limit load. Table 3.5 shows the calculated values for each tank.

3.3.3 Thermal Design

The thermal design of the tank is essential for the success of the mission and the overall design. Thermal losses due to huge temperature gradient directly affect to the global efficiency of the mission as well as to the range of the aircraft. In order to prevent excessive boil-off of the LH_2 propellant, an effective insulation of the tank is required. Thus, one-dimensional steady-state model based on the electrical resistance analogy has been performed in order to estimate the heat flux leakage. Equation 3.2 states the calculation of the heat flux, which depends on internal and external temperature and the equivalent resistance.

$$Q = \frac{T_{air} - T_{LH_2}}{R_{equi}} = \frac{T_{air} - T_{LH_2}}{\sum R_i} \tag{3.2}$$

where R_{equi} is the total resistant resulting of the summation of both internal and external natural convection and also both conductivity resistances of the tank wall and coating. Due to non-integral tank configuration, external natural convection has been applied, since the outer wall of the tank is not in contact fuselage surface. As both temperatures are known during the flight (It's assumed that temperature inside the fuselage is the same as outside temperature), the only missing parameters would be the value of each resistance. It is important to remark that an extra 30% of heat transfer have been added due to the unconsidered losses of the model related with supports, connections, simplifications and the piping [38].

Natural Convection For external natural convection, the correlation of George D. Raithby and K.G. Terry Hollands [43] for horizontal cylinders has been used to calculate Nusselt number, whereas for internal convection a different approach has been adopted. As hydrogen is present in two phases (gas and liquid), a different correlation has been implemented for each phase. For gas phase, Churchill and Chu correlation has been selected [44], since it takes into consideration the destabilised of the boundary layer for laminar and turbulent regime. For the liquid, the correlation suggested by [44] was used, where both the Nusselt and Rayleight numbers are based on the height of the liquid phase. As the fraction of vapor-liquid is changing over the flight, total internal heat coefficient is calculated as follows:

$$h_{in} = \frac{1}{S_w}(h_{in,gas}S_{w,gas} + h_{in,liquid}S_{w,liquid}) \tag{3.3}$$

Conduction The resistance due to conduction has a major influence on the heat flux due to the low conductivity of the insulation foam. As this conductivity depends on temperature, the mean temperature between both surfaces of the coating has been used to determine the conductivity.
An iterative calculation should be performed to get both external and internal heat transfer coeffi-

Table 3.5: Geometric parameters

Parameter	Unit	Inner	Middle	Outer
Storage volume	[m^3]	84.6	37.9	14.7
Inner radius	[m]	1.44	1.05	0.74
Insulation thickness	[cm]	20	20	20
Wall thickness cylinder	[mm]	3	2	1.5
Wall thickness spherical heads	[mm]	1.5	1.2	1
Length	[m]	13	11.1	8.6
Mass	[kg]	2630	1880	1470

cients. Once both are calculated, the total resistance is obtained an so, the heat flux for different thickness of the coating. As the effective thickness for the tank has to be found, a parametric study variation the insulation thickness has been performed. A schematic model of the detail calculation process presented in Appendix E.1.

3.3.4 Results

The final choice of the insulation thickness for each tank is based on the compromise between maximizing the volume, taking into account the losses due to boil-off, and minimizing the weight. Adding more insulation thickness results in the one hand in a reduction of boil-off losses, but on the other hand it is decreasing the usable volume as well as adding weight. The mission profile determines the required fuel mass m_{req}, if a certain mass m_{vent} is vented, additionally storage is needed, therefore the total fuel mass needed is the sum of those. The dimensionless parameter $r_m = m_{req}/m_f$ therefore evaluates the efficiency of the insulation and quantifies the losses due to boil-off. To evaluate a mass-based efficiency of the system the dimensionless parameter $\eta = m_f/(m_f + m_t)$ is introduced, to evaluate a mass-based efficiency. The product of η and r_m is the overall efficiency of the fuel system η_{req} [40]. Additionally a vapor cooled shield (VCS) is installed, which reduces boil-off rates significantly. The VCS consists of a spiral tube inside the insulation, where evaporated hydrogen swirls around the tank, absorbing some of the heat leakage and thus reducing boil-off losses by up to 60% [45], thus achieving efficiency values for $r_m = 0.988$, $\eta = 0.77$ resulting in an overall efficiency of $r_m = 0.988$.

3.4 Aircraft Cabin Design for Global Market

Since the aircraft design process is a delicate balance of various facets, the cabin layout as an integral part of the overall concept targets not only the structural weight minimization, but also numerous other requirements such as ensuring a safe evacuation and seamless ground operations [46].

3.4.1 Passenger Experience

Improvements were made taking both the passengers comfort and the aim of reducing weight on the part of the airlines into account. While providing safety and comfortable support are still the main functions of the passenger cell the flight experience three decades from now will look differently, not just the cabin itself, which is affected by the current revolutionary aircraft configuration, but also how the passenger perceives it. Due to the fact that physical mock-ups are very cost-intensive and complex acceptance tests with regard to future cabin concepts are difficult to conduct [47], the present cabin offers maximized space to implement more flexible cabin design adapting to the dissolution of traditional cabin compartments [48]. As mentioned above the centerbody contains five separated longitudinal tubes where all passengers are seated on one deck. Due to the configuration characteristics and because of weight-saving measures a windowless design is implemented. In order to avoid any claustrophobical feeling or an uncomfortable condition on the part of the passenger high fidelity displays are embedded into the side wall showing images captured by an outboard camera. As the total absence of windows is one of the most challenging issues concerning the passengers acceptance, existing airplane's window holes can first be replaced by hidden screens

to make the passenger get used to the windowless concept.[49] The elaborated cabin layout is illustrated in 3.8. In the forward area 8 lavatories, 40 FST, 6 HST and 136 SU are integrated. In order to ensure a safe evacuation 6 cabin attendant seats are each provided in the front and aft fuselage. In case of supplying additional passenger service the number can be adjusted. The center part provides a total seating capacity of 531 in the all-economy configuration (7 additional seats compared to the B747-400ER) with a seat width of 18" at 33" pitch combined with an 7" recline while offering the additional possibility to implement common two- or three-class seating options. The aft fuselage houses 4 lavatories, 22 additional FST and 60 SU. As an efficient turnaround is an integral part of airline's success it is necessary to keep maintenance as simple as possible. For this reason, a spatial mixing of seating, toilet and galley area is avoided, which additionally increases the passenger comfort due to reduced noise level. With a focus on very high passenger convenience the customizable seats offer amenities like additional stowage, advanced ergonomics, in-seat power supply and Bring Your Own Device (BYOD) integration. To suit the needs of the passenger especially on long-distance overnight flights an advanced chronobiologically-adapted cabin lighting system is integrated to improve the wellbeing and reduce jet lag [50]. A detailed view of the cabin layout is presented in fig Appendix L.4 and Appendix L.5.

Figure 3.8: Cabin layout

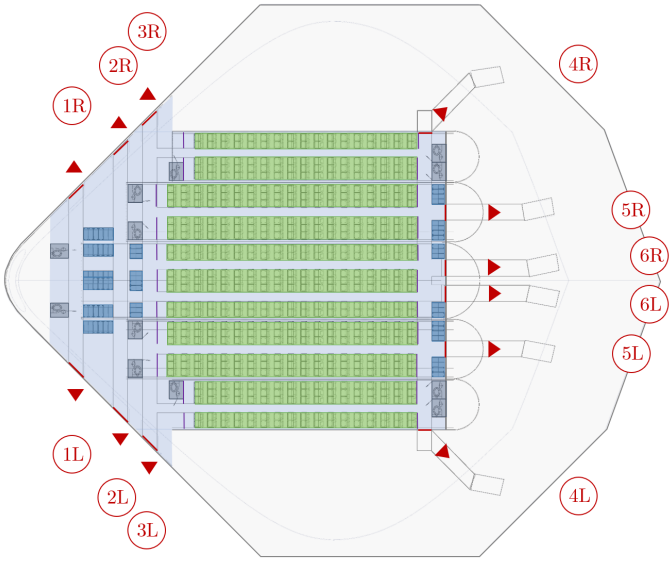

3.4.2 Cargo Compartment

The cargo compartment is located in the underfloor of the passenger cabin. The type of freight commodation varies depending on the cargo hold height. In the middle tube, the storage of cargo in 14 LD3-45 containers is ensured. Due to the lower load compartment height, only the use of 26 PKC pallets is possible in the two inner tubes [51]. In the two outer tubes, the accommodation of bulk cargo is possible. Overall, the cargo hold offers maximum load capacity of 150 m^3, with offering 11 m ^{3} more than the B747-400ER.

3.4.3 Emergency Evacuation

As required by the airworthiness authorities at least the safety standard demonstrated in existing aircraft must be guaranteed for the certification of new aircraft types. To fulfill the requirements the maximum distance of 60ft between two exits is complied with. For all airplanes with a capacity of more than 44 passengers it must be demonstrated that all occupants, including crew members, can evacuate the cabin within 90 seconds with not more than half of the exits available [52]. This test shall be performed using an agent-based egress simulator which is designed to reproduce evacuation scenarios. Based on the cabin layout a simulation model is created including the main components, such as aisles, seats, doors and evacuation slides. According to the Certification Specifications the

passenger load requires 5 Type A exits on each side of the cabin. However, an additional exit pair is needed in this design, in order to comply with the required maximum evacuation time. For the evacuation a representative passenger load is considered as specified in the Appendix J of the CS-25 (see Appendix M). In order to comply with these regulations the profiles *Man*, *Woman*, *Old Woman*, *Old Man* and *Mother* are created. These profiles are characterized by walking speeds and waist sizes with regard to sex and age group (see Appendix D.1). Since the movement of an occupant is restricted in the legroom between the seats, a speed modifier of 0.5 is imposed. In addition, an initial delay at the beginning of the evacuation is considered in order to simulate the seat belt release and reaction time. Movement conflicts and collisions between the occupants are taken into account. The simulation model before and during the evacuation process is shown in the figures 3.9 and 3.10.

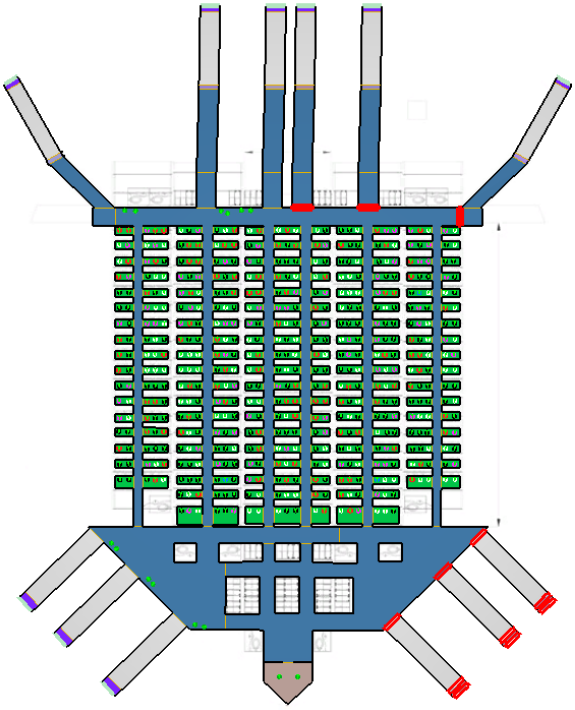

Figure 3.9: Initial simulation configuration

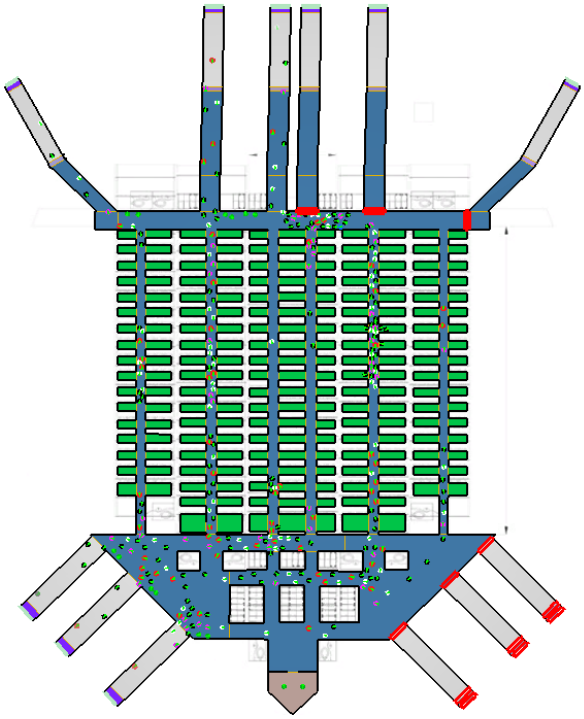

Figure 3.10: Configuration during evacuation

With the shown model 20 simulation runs are performed. The average values for evacuation time and flow rates are shown in table 3.6.

Table 3.6: Evacuation simulation data

Exit	**1R**	**2R**	**3R**	**4R**	**5R**	**6R**
Flow rate [PAX/s]	1.48	1.47	1,32	0.74	1.18	1.35
Evacuation time [s]			82.3			
Std. deviation [s]			2.16			

For Type A exits a reference value of 1.675 PAX/s can be considered [53]. Although the obtained exit flow rates in the simulation model are smaller than the reference value, the cabin was evacuated within 90 seconds using only 50% of the exits. Nevertheless, the evacuation of a BWB constitutes a novelty in the aviation industry which may require amendments in terms of the certification criteria.

3.4.4 Ditching

Although ditching is extremely rare in modern aviation, this case has to be considered in the certification process if requested. Due to the fact that the ditching behaviour cannot be simulated it has to be examined on the basis of model tests or with the help of reference aircraft configurations

with known ditching characteristics. The current configuration is in accordance with the requirements of CS 25.801(i) and the entire equipment demanded in CS 25.1415 is available. [52] During the ditching event the centerbody has to withstand high pressure loads, with blended wing-body configuration offering a better crash performance over classic tube-and-wing configurations. Additionally the engine installation at the rear has the advantage that passengers are protected from injury as well as the engines themselves are shielded from fragments [54].

4 Aircraft Characteristics

Where the previous chapter explained the interaction of the components, this chapter is focused on the capabilities of the BWB as a whole. Therefore, the potential mission profiles will be assessed, the mass will be broken down into single fractions, flight mechanical considerations are made and the performance requirements are examined.

4.1 Mission Profile

The mission profile divides the mission into segments which are characterized by constant atmosphere and performance parameters. Hence, each segment can be represented by average parameters which provide appropriate results regarding the conceptual design phase.
For the following design process, two related mission profiles are considered. The first represents the typical design mission according to the CEAP LTO-cycle. Based on this, energy calculations and ground handling applications can be conducted. The second profile additionally covers all alternate and exceptional cases, which can occur during the flight. Hence, it describes the worst case mission, which constitutes the foundation for the fuel mass determination and the tank dimensioning. Both profiles are collectively shown in figure 4.11. The performance data will be shown for each segment

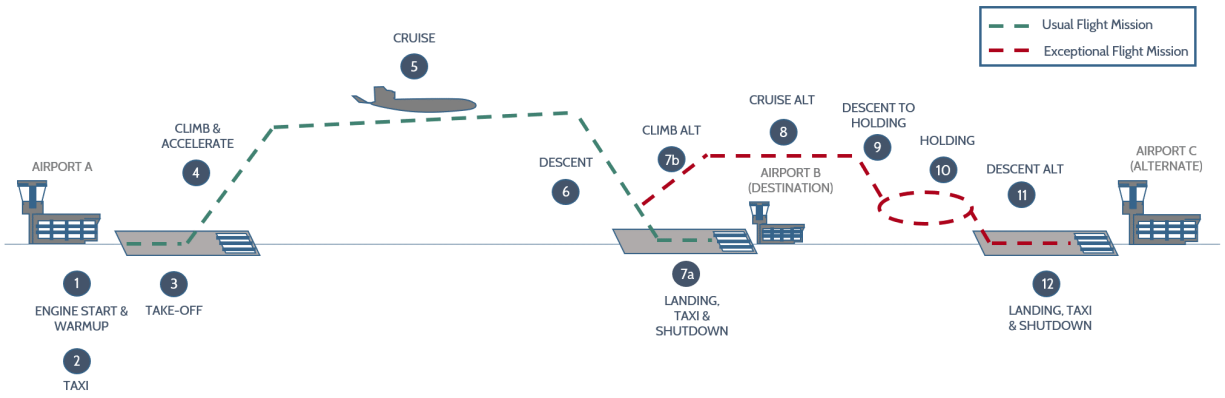

Figure 4.11: Design mission profile

of the profiles in section Appendix J.

4.2 Mass determination

The mass determination is divided into fuel mass and an overall mass breakdown. Both are based on conventional design methods, which are adjusted to the blended wing configuration and hydrogen as fuel.

4.2.1 Fuel Mass Fractions

The fuel mass is a critical factor in the design process that facilitates comparisons of energy consumption (see section 6.1) and the tank design (see section 3.3.1). It is mainly based on a modified fuel fraction method referring to Roskam's [55]. Therefore, several suggested Roskam fuel fraction factors RFFF are assigned to each mission phase being similar to the mission profile segments from

section 4.1. In order to match the real masses of the B747-400ER the chosen RFFF deviate from the original ones. Usually the factors apply to conventional jet engines burning kerosene. Since the propulsion's physical principal remains the same, as stated in section 3.2.1, the application of a hydrogen adjusted Roskam method is legitimized. The combination of modified fuel fraction factors ($\mathrm{MFFF_{H2}}$) and the Breguet formula delivers a proper fuel mass determination for this special configuration. Section Appendix J provides an overview of the calculation method which the fuel mass of each mission segment is calculated with. Both modifications are discussed in the following paragraphs.

H2-Modification of Fuel Fraction Factors For each segment (design: $j = 1...7a$, worst case: $j = 1...12$) the RFFF is defined as shown in equation 4.4 left. The goal of the modification is to achieve an equivalent fraction factor which is valid for hydrogen, such as in equation 4.4 right.

$$\mathrm{RFFF}_j = \frac{m_{\mathrm{K,End},j}}{m_{\mathrm{K,Start},j}} \qquad \mathrm{MFFF}_{\mathrm{H2},j} = \frac{m_{\mathrm{H2,End},j}}{m_{\mathrm{H2,Start},j}} \tag{4.4}$$

Therefore, the calorific equivalent for each phase of the mission can be compared with the quotient:

$$\frac{m_{\mathrm{H2,Start},j} - m_{\mathrm{H2,End},j}}{m_{\mathrm{K,Start},j} - m_{\mathrm{K,End},j}} = f_{\mathrm{KtoH2}} \tag{4.5}$$

In the equation, the calorific equivalence factor represents the ratio between the inferior heating values of both fuels: $f_{\mathrm{KtoH2}} = \frac{H_{i,\mathrm{K}}}{H_{i,\mathrm{H2}}}$.
The corresponding mass must be equal to the difference between the start and end mass of each segment, because the only weight loss is caused by consumption of fuel. Because hydrogen has a higher calorific value than traditional fuels like kerosene, less is needed to obtain the same energy yield. The question remains, to what extent will hydrogen fuel affect the start and end mass of each mission phase. Using the takeoff mass as an initial iteration value, the following two cases may arise:

a. The start mass decreases (while the end mass remains constant) for each segment preceding take off.
b. The end mass increases (while the start mass remains constant) for each segment following take off segment including the take off mission itself.

These assumptions result in the following modified fuel fraction factors for hydrogen at each respective mission segment:

$$\mathrm{MFFF}_{\mathrm{H2,a},j} = \left(f_{\mathrm{KtoH2}} \cdot \left(\frac{1}{\mathrm{RFFF}} - 1 \right) + 1 \right)^{-1} \tag{4.6}$$

$$\mathrm{MFFF}_{\mathrm{H2,b},j} = 1 - f_{\mathrm{KtoH2}} \cdot (1 - \mathrm{RFFF}) \tag{4.7}$$

Equation 6.15 may be used to calculate the $\mathrm{MFFF}_{\mathrm{H2},j}$ prior to take off and equation 6.15 after the take off segment.

H2-Modification of the Breguet formula Breguet's range formula can be used to calculate a fuel fraction factor for climb and cruise phase for which sufficient data is available. For the take off and descent phase the fuel fraction factor by Roskam is used.
The equation can be formulated as a fuel fraction (see equation 4.8).

$$\frac{m_{\mathrm{Ende}}}{m_{\mathrm{Start}}} = e^{-\frac{SFC \cdot \varepsilon \cdot g}{v}} \tag{4.8}$$

Because the SFC is the only parameter related to the mass of kerosene, an adjustment is required. Similarly, the calorific modification above is valid:

$$SFC_{\mathrm{H2}} = SFC_{\mathrm{K}} \cdot f_{\mathrm{KtoH2}} \tag{4.9}$$

For the cruise and climb segment specific fuel consumptions for kerosene SFC_{K} can be calculated with the help of the approximation of Torenbeek [56]. Table Appendix G.1 provides the required engine parameters. As specified by equation 4.9, the resulting values are $SFC_{\mathrm{H2,CR}} = 0.1460 \frac{\mathrm{kg}}{\mathrm{daNh}}$ and $SFC_{\mathrm{H2,CL}} = 0.1995 \frac{\mathrm{kg}}{\mathrm{daNh}}$ with which the Breguet fuel fraction factors ($\mathrm{BFFF_{H2}}$).
All adjusted fuel fraction factors are listed in section Appendix J. Besides, further modification of the SFC and $\mathrm{MFFF_{H2}}$ regarding any fuel savings is considered in section 6.1. Accordingly, the values for any hydrogen fuel mass already include the savings.

4.2.2 Mass Breakdown

An accurate mass prediction at the preliminary design stage is essential for the proper calculation of the Maximum Take Off Mass (MTOM), a design parameter of utmost importance. The semi-empiric weight prediction method according to Torenbeek delivers adequate results at early design stages [56]. To provide the necessary comparability, both the baseline and the new conceptual airplane are calculated with this method, apart from a few exceptions which are specified below. The main difference between the BWB and the B747-400ER is the centerbody. To get a first weight estimation the equations in "A Sizing Methodology for the Conceptual Design of Blended-Wing-Body Transports" can be used [57]. The centerbody is composed of a pressurized passenger compartement and an aft non-pressurized section which is used to support the engines. The wing part can be calculated derived by Torenbeek. The pressurized passenger compartment has the weight of the fuselage and is calculated as follows:

$$W_{fuse} = 5.698865 \cdot 0.316422 \cdot (MTOW)^{0.166552} \cdot (S_{Cabin})^{1.061158} \tag{4.10}$$

In the equation MTOW is the maximum takeoff mass and S_{Cabin} the planform cabin area. This equation and the constants were developed with a finite element analysis. The aft non-pressurized section can be calculated with the following equation:

$$W_{aft} = (1 + 0.05 \cdot N_{Engines}) \cdot 0.53 \cdot S_{aft} \cdot MTOW^{0.2} \cdot (taperRatio_{aft} + 0.5) \tag{4.11}$$

Where $N_{Engines}$ is the number of engines. The detailed mass breakdown can be found in Appendix B. With 201,003 kg the operating empty mass is about 10% higher compared with the operating empty mass of the B747-400ER which is a result of the different tank design. A consequence of the the new BWB tank design are additional mass fractions, and therefore a higher operating empty mass, due to the required cooling system which causes an increase of the airframe structure weight by 10% compared with the B747-400ER. The BWB has a MTOW of 289,994 kg.

4.3 Performance

The mission performance capabilities consist of start, climb, cruise and landing performance. Each is dictated by the mission performance of the B747-400ER as a minimum requirement. All performance calculations are carried out assuming standard conditions for pressure, temperature and density (ISA).

4.3.1 Take off and Cruise

By matching the take off thrust requirement and the cruise thrust requirement the necessary thrust to be installed can be configured. In addition parameters, such as wing loading, lift coefficient, drag to lift ratio and initial cruise altitude (ICA) are either calculated or obtained from literature. A calculation method for both requirements is provided by the chair of Aircraft Design and Aerostructures of the TU Berlin. The principle is illustrated in figure 4.12.
The method suggests that the static thrust to weight ratio for take off is modeled as a function of a variable which runs from 0 meters to the take off field length (TOFL). As required the TOFL is equal to the reference case (see table 2.2). Furthermore the scenario of a single engine failure during take off must be accounted for in accordance the CS-25. In order to set the engine failure recognition speed the optimization concept of the Balanced-Field-Length is applied.

The required static thrust to weight ratio during cruise results from equilibrium of forces in a stationary horizontal flight state.
After plotting both functions (see 4.12), the thrust matching can be performed. As shown in figure 4.12 the functions depend on a variety of parameters. The assumptions for these parameters are discussed in the following paragraphs.
Value ranges for the aerodynamic parameters, which can be derived from literature, are considered as follows:

- Lift coefficient for take off: 1.1-1.3 [58], [59], [18]
- Lift to drag ratio for take off: 8-12 [58], [59], [18],
- Lift to drag ratio in cruise phase: 23-26 [58], [59], [18]

These ranges will need to be adjusted during the iteration process. Chapter 3.1.2 demonstrates that CFD methods are useful to obtain values which can be applied to this design process.
The wing loading of a BWB is typically lower compared to conventional aircrafts with similar dimensions. This is related to a rising surface area, whereas weight remains nearly constant. The literature provides a value range of approximately 2,500-4,000 N/m^2 [58], [59], [18]. As an initial value for the iteration a lower wing loading for take off was set. This is due to the necessity of a high total surface area which is divided into the wing and center body area. A considerable part of the surface area is already covered by the center body due to the high volume requirements of the tank and cabin. To ensure that the outer wing has a sufficient wing span, the remaining wing area must be adjusted in accordance with the chosen wing parameters in chapter 3.1.2. This directly affects the total wing area. The high surface area also leads to high friction drag which must be compensated by an increase of the initial cruise altitude. In order to achieve a balanced propulsion design, the ICA must be restricted by the minimum required thrust for cruise.
Because the thrust directly affects the engine weight, it is desirable to minimize the required thrust. Figure 4.12 illustrates that the static thrust to weight ratio is matched between take off and cruise phase at its possible minimum. In table 4.7 the final parameters resulting from the thrust matching are summarized. The lift coefficient in cruise, which derives from the horizontal flight condition,

Table 4.7: Final thrust matching data

Parameter	Value
Required static thrust to weight ratio [-]	0.253
Installed static thrust [kN]	717,067
Take off	
Wing loading $\left(\frac{W}{S}\right)_{\mathrm{TO}}$ [N/m^2]	2,173
Lift coefficient $C_{L,\mathrm{TO}}$ [-]	1.1
Lift to drag ratio $\left(\frac{L}{D}\right)_{\mathrm{TO}}$ [-]	12
Thrust [kN]	534,664
Cruise	
Initial Cruise Altitude [m]	11200
Lift to drag ratio $\left(\frac{L}{D}\right)_{\mathrm{ICA}}$ [-]	23
Thrust [kN]	120,768

equals to 0.194 at an angle of attack of approximately 4° (see figure 3.5).

4.3.2 Climb

The climb thrust requirement is not taken into account in the propulsion dimensioning assuming that the installed thrust, which is calculated above, fulfills this climb thrust requirement. Hence, it is necessary to check wether the climb performance capabilities of the baseline comparison can be reached. Therefore, a climb performance, in terms of a mean climb velocity, is approximately

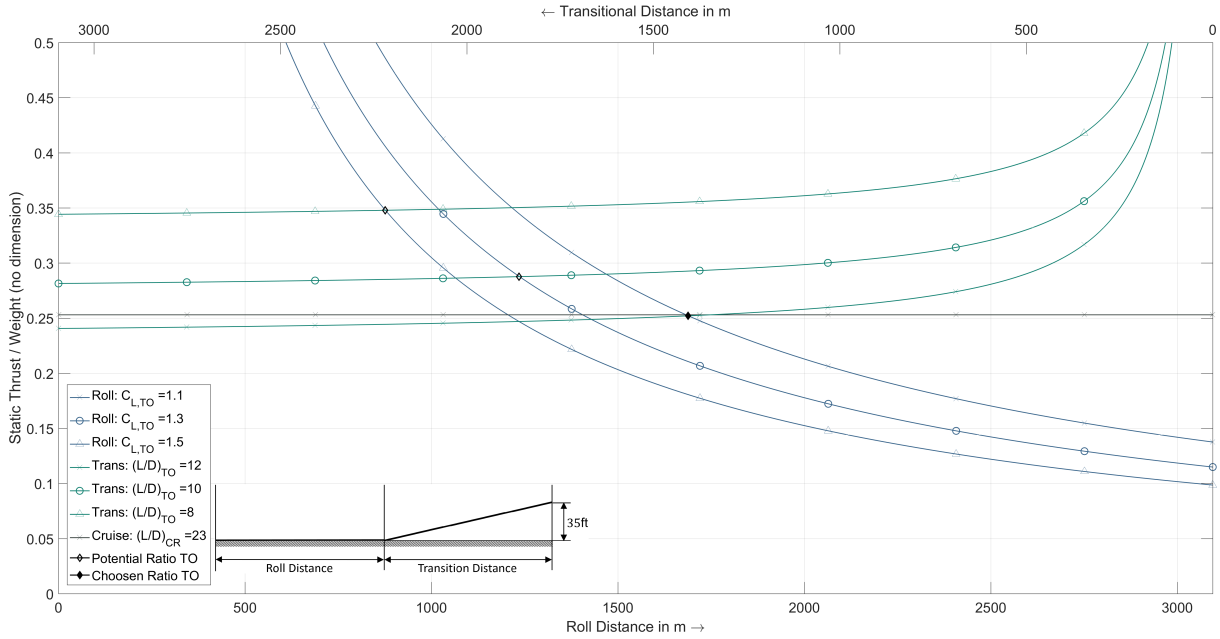

Figure 4.12: Thrust matching between take off and cruise

determined as follows:

$$\overline{w}_{CL} = SET \cdot v_{CL} = \left[\frac{T_{CL}}{\overline{W}_{CL}} - \varepsilon_{CL}\right] \cdot v_{CL} \tag{4.12}$$

Besides, the knowledge of the specific excess thrust (SET), which consists of the difference between thrust to weight ratio and drag to lift ratio for climb, is essential. The ratio is calculated with the installed static thrust (see previous section), which must be modified by taking inlet pressure losses and performance map induced losses into account. Dividing the required thrust for climb by the mean climb weight equals the required ratio. Furthermore, in conceptual design phase the following estimation can be used:

$$\varepsilon_{CL} = 1.1 \cdot \varepsilon_{CR} \tag{4.13}$$

Under consideration of all assumptions the mean climb velocity is 5.32 m/s (with a SET of 0.0303), while the reference aircraft provides a mean climb velocity of 8.04 m/s [60]. It is shown that the required climb performance is surpassed.

4.3.3 Landing

Two restrictions will define the landing segment of the mission profile. The first requires that the available landing field length is not exceeded. According to the second restriction the approach speed must be 30% higher than the stall speed while preparing to land. Both restrictions will limit the maximum landing wing loading and can be found in table 2.2. The maximum values were obtained from the drag to lift ratio and the lift coefficient for landing. The value ranges extracted from the literature are written below:

- Lift coefficient for landing: 1.2-1.5 [58], [59], [18]
- Lift to drag ratio for landing: 8-10 [58], [59], [18]

Table 4.8 contains the maximum values with respect to both restrictions, the corresponding aerodynamic parameters and the wing loading calculated.
Comparing the values it can be noted that both restrictions are respected.
High lift devices are required to fulfill the aerodynamic parameters (see 3.1.3), to achieve the necessary take off and landing performance. This becomes clear when comparing the lift coefficient

Table 4.8: Final thrust matching data

Parameter	Value
Max. Wing loading (due to landing field length) $\left(\frac{W}{S}\right)_{\mathrm{LD,max,1}}$ [N/m^2]	2,0329
Max. Wing loading (due to approach velocity) $\left(\frac{W}{S}\right)_{\mathrm{LD,max,2}}$ [N/m^2]	2,469
Wing loading $\left(\frac{W}{S}\right)_{\mathrm{LD}}$ [N/m^2]	2,013
Lift coefficient $C_{L,\mathrm{LD}}$ [-]	1.2
Lift to drag ratio $\left(\frac{L}{D}\right)_{\mathrm{TO}}$ [-]	10

polar in figure 3.3 with the chosen values.

5 Feasibility

A highly performant system, such as the introduced one requires an adapted thought through airport infrastructure to deliver the ecological benefits, economical advantages and reduced impacts of the environment, it is capable of. After mentioning the integration into existing systems, selected adaptions are displayed here.

5.1 Assimilation to Existing Systems

Today's ground procedures are highly optimized for present aircraft configurations and infrastructure [61]. Although the presented concept is disruptive at many levels the implementation into existing systems is considered. One aspect is ground handling which is explained in the following and displayed in figure 5.13. There is not much change to the existing procedures: Passengers board the plane from one side (using up to three gangways) while maintenance and service vehicles approach from the opposite. Cargo applications are separated from passengers entry, approaching the aircraft mostly from behind. Table 5.9 shows all service positions and their respective numbers. Arrows implicate a further movement under the body and then reaching for cargo doors from behind (bulk and baggage cargo loaders) or the nose wheel from the front (TaxiBot - explained below). With further improvement of ground procedures, highly efficient turn around times can be achieved, reducing CO_2 even more and optimizing the airports as bottleneck of modern Air Traffic Management (ATM) [62].

Table 5.9: Service positions

Nr	Service Position	Nr	Service Position
1	Gangways	5	Cabin Cleaning Vehicle
2	Bulk Cargo Loader & Trailer	6	TaxiBot
3	Galley Service Vehicle	7	Fuel Service
4	Baggage Cart (Cargo Loading)	8	Cart with LD3-45

5.1.1 TaxiBot

As a disruptive approach for ground manoeuvring and taxiing the TaxiBot is introduced [63]. It is capable of lifting the front wheel up, pushing the aircraft and drive it to the runway holding point without any modifications necessary to the aircraft [64],[65]. After the push back the pilot takes control over the bot (Pilot Controlled Mode [66]), using it instead of the aircraft's wheels, brakes and engines [65] leading to reduced fuel burn (by 85 %), gas emissions (by 85 %) and noise (by 50 %) [64]. Furthermore, the bot's fuel consumption varies from 2-5 % the amount of taxi fuel used by an Boeing 747 [67] or A380 [63]. Till 2045 the propulsion concept is expected being fully electric and providing electric, pneumatic and hydraulic power for the aircraft. As a result of the power supply by the TaxiBot an APU is expendable. Due to higher mass and friction, the TaxiBot provides more traction on slippery or icy surfaces resulting in optimized ground operation safety [66].
To maximize the advantages of the TaxiBot-system, it should be implemented first at hub airports

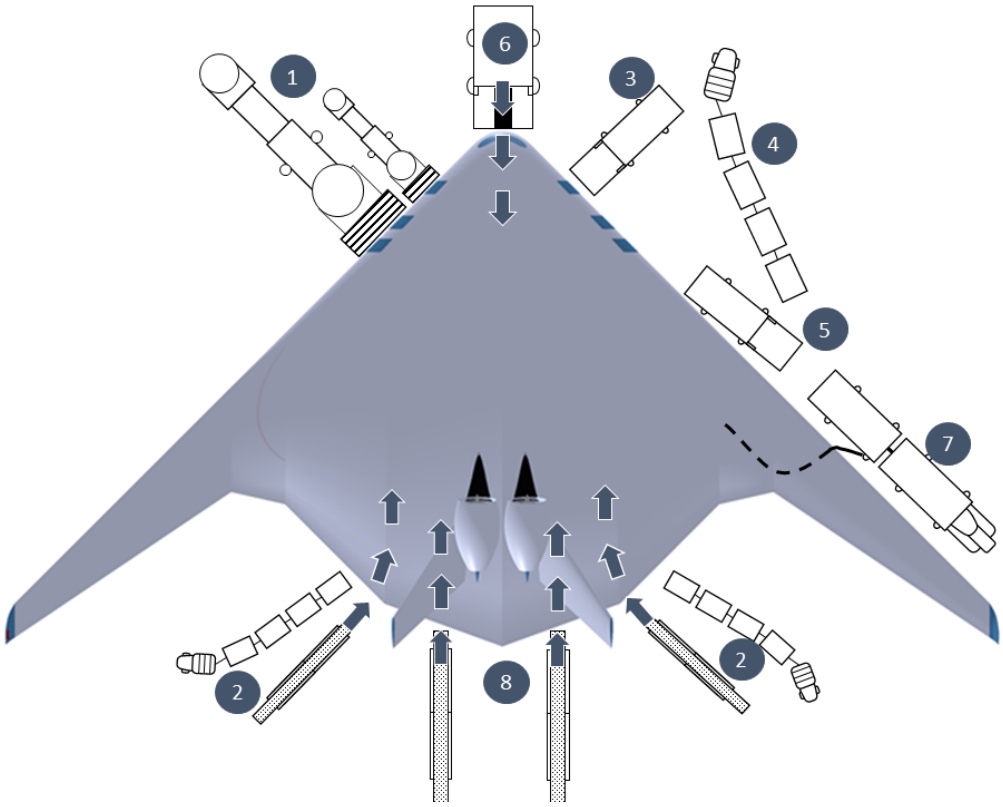

Figure 5.13: Ground handling

with high taxi out times and high occupancy rates to improve efficiency and reduce block time [66]. Although it is possible to use the TaxiBot for taxi-in procedures, those are likely to be more complicated because it is logistically difficult to connect a TaxiBot on the taxiway [66].

5.2 Airport Infrastructure

The use of liquid hydrogen as aviation fuel comes with challenges, regarding the airport infrastructure, respectively distribution and storage. In order to maintain the aircraft, hydrogen supply must be guaranteed on the airport. For distribution there are three different approaches.a) Transport of liquid hydrogen b)Transport of gaseous hydrogen and liquification at the airport or c) on-Site Production and liquification. Ideally, hydrogen would be produced and liquified directly at the airport in order to eliminate transportation costs and losses. Implementation of this on existing airports will require expensive adjustments and will be most likely limited due to space restrictions [38]. The remaining methods, namely liquid or gaseous transport are obviously connected with efficiency losses, respectively additional costs due to boiloff and/or transportation. For gaseous transport and onsite production hydrogen needs to be liquified on the airport site. Furthermore a significant amount of liquid hydrogen needs to be stored for possible fluctuations in the demand from aircraft [38]. For storage applications, spherical tanks are suggested by several studies as they provide the best volume to surface ratio as well as the best resistance to stresses caused by pressure. To provide maximum efficiency, the biggest Hubs are adapted for the use of hydrogen with an onsite production via electrolysis as well as liquification. The liquid hydrogen is then stored in large spherical cryotanks. Sub-cooled liquid hydrogen is then delivered through insulated pipelines under the ground to fuel the aircraft. In An approach to connect hydrogen supply for aviation as well as for automobile traffic could offer further synergies.

5.3 Consideration of Emergency Cases

Considering general safety aspects of handling and using hydrogen for aviation, studies have shown that the overall safety level is at least as high as when using kerosene, on the provision that safety

procedures are strictly observed [68].
It is commonly believed that the handling of a hydrogen-powered aircraft is similar to a conventional aircraft, when it comes to fueling, boarding and cargo loading. Besides, turnaround times are expected to not drastically change. In order to avoid boil-off losses the cryogenic temperatures of the tank must be maintained. During maintenance periods the hydrogen tank needs purging before being refueled again [69].
In order to preserve safety during operation ventilation is required which avoids accumulations of hydrogen outside of the tank. The occurrence of leakage is less critical than with other fuels, as it evaporates into the atmosphere fast enough to avert critical conditions. The tanks show a high robustness and therefore are less likely to break in case of a crash. Furthermore, ignition of hydrogen cannot be triggered by impact in a crash situation. However, thorough testing and checks must be performed in order to detect and asses the severity of leaks [38].

6 Sustainability

The aspect of sustainability is essential in order to achieve long term solutions in the aviation industry. For this it is necessary to seek a compromise between economic interests, the preservation of the environment and human needs.

6.1 Energy Consumption

Corresponding to section 2.2 a total energy reduction of at least 60% is one of the design study's main target. Since the BWB configuration including its aircraft characteristics is known, a first approach will be formulated in order to determine the energy consumption.
The first law of thermodynamics states that „The change in energy of a system is equal to the difference between the heat added to the system and the work done by the system".[70] Considering that burning fuel is the only supply of energy to the system, the energy consumption can be derived from the calorific potential of each fuel. Therefore, the inferior calorific value or the inferior heating value, is defined as „The amount of heat which would be released by the complete combustion in air of a specified quantity of gas [...]". [71] Hence, with the knowledge about the fuel consumption of each segment as it is calculated in section 4.2.1, the energy consumption for each aircraft can be determined and a comparison between both can be drawn. Prior to that, it is necessary to consider all assumed savings from table Appendix C.1. Therefore, the fuel fraction factors, which are already adjusted to the combustion of hydrogen, reiceive a further modification concerning the fuel reduction benefit (FRB). The implementation of the FRB's is divided into the different types of benefits and will be discussed as follows. All aerodynamic improvements are represented by the assumed lift to drag ratio of 23 (see 4.3.1). The ratio is incorporated in the formula of Breguet (see equation 4.8).

Usually all engine improvements are reflected in the specific fuel consumption. However, the SFC approximation of Torenbeek (see section 4.2.1) only takes parameters into account which are specified in table Appendix G.1. Hence, the fuel reduction benefits induced by features like the GTF, VPF, BLI, fan improvements and bling-concept, are merged to an engine feature benefit (EFB) of 38.65 %. Every single feature benefit can be found in section 3.2. Similarly to equation 4.5 the following quotient is formulated:

$$\frac{m_{\text{New,Start},j} - m_{\text{New,End},j}}{m_{\text{Old,Start},j} - m_{\text{Old,End},j}} = (1 - (EFB)) \tag{6.14}$$

The index „New" indicates the EFB, whereas the index „Old" just represents the modification from

kerosene to hydrogen. This approach leads to improved fuel fraction factors (IFFF).

$$\mathrm{IFFF}_{\mathrm{a},j} = \left((1 - \mathrm{EFB}) \cdot \left(\frac{1}{textMFFF_{\mathrm{H2,b},j}} - 1 \right) + 1 \right)^{-1} \tag{6.15}$$

$$\mathrm{IFFF}_{\mathrm{b},j} = 1 - (1 - \mathrm{EFB}) \cdot (1 - textMFFF_{\mathrm{H2,b},j}) \tag{6.16}$$

Again both cases (prior to and following take off segment) are considered.
Mission optimization leads to a TaxiBot described in 5.1.1. As described, the consumption of a taxi with the bot compared to an usual taxi is assumed to be 5%. Thus, the equivalent taxi fuel mass is calculated based on an taxi fuel fraction factor (TFFF). TFFF is derived from the hydrogen-modified TFFF which is improved by the taxi bot benefit of 5%. The equivalent improved hydrogen mass is transformed into an equivalent hydrogen energy which equals the bot's electric energy for one taxi phases.
Furthermore, the reduction of any mass always is advantageous in terms of an decreased fuel consumption. Due to the cumulative effect a local reduction of mass is always affecting further mass losses. It is clear, that the whole process is iterative. Eventually, the targeted energy reduction is surpassed, as this design reaches a value of 62.2% compared to the reference case. The energy of each segment is provided in section Appendix J
So far, the energy determination is largely based on the propulsion energy. Especially the formula of Breguet does not include the consumption of electrical devices which the aircraft is equipped with. Since this is also not considered for the B747-400ER the relative improvement in energy consumption should nearly remain the same. Nevertheless, it is shown in former sections that the potential can rise up to 80%. For instance engine concepts like IRA or the drag and mass benefits of the ADHF were not taken into account yet and might yield a further savings potential.

6.2 Environmental Impacts

Through engine emissions and noise aircraft operation causes direct impacts on the environment. These two issues are the main driving forces in technology research. In order to comply with the goals set by ACARE in Flightpath2050 (75% CO_2 and 90% NOx) [8], tremendous changes are needed.

6.2.1 Emissions

Although there is a permanent improvement in fuel efficiency, the growth in passenger air traffic is rising consequently, overcompensating the reduction in average fuel burn per passenger kilometre. In 2012, aviation made up 3% of the total EU CO_2 emissions and 7% of the total EU NOx emissions . It is assumed that CO_2 and NOx emissions will increase by 44% and 42% until 2035, taking into account a reduction of 46% of average fuel burn (kg) per passenger kilometer [72]. The substitution of kerosene with hydrogen constitutes a suitable option for the preservation of the environment. In figure 6.14 the combustion products of kerosene and hydrogen are listed. The effect of the major

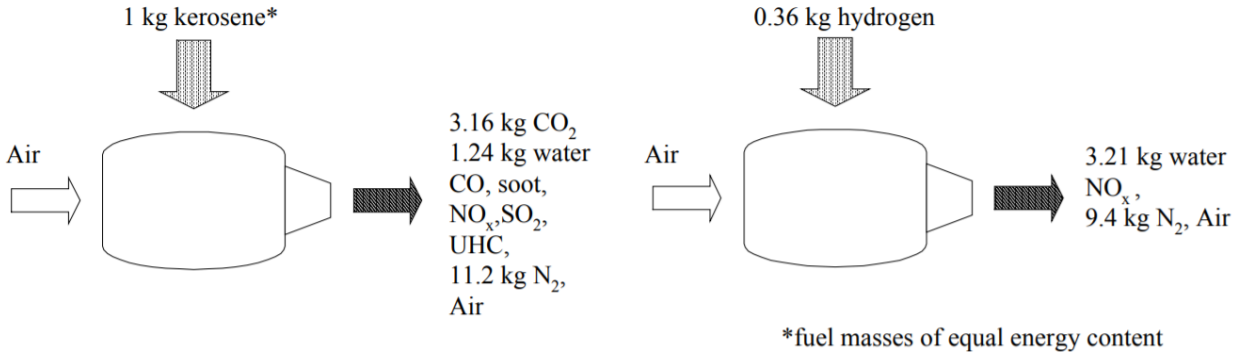

Figure 6.14: Combustion products of kerosene and hydrogen [16]

exhaust products of kerosene and hydrogen combustion (CO_2, NOx and water vapor) in dependence of the altitude is shown in Appendix F.1 (derived from Seeckt [73]). Water vapor is the most abundant and dominant greenhouse gas in the atmosphere, its global warming potential strongly depends on the altitude [74]. The global warming potential (GWP) is calculated by determining the fuel mass flow for each segment and relate it to its altitude dependent impact. The definition of mission segments with the corresponding fuel consumption and altitudes as well as the time increment is given in section Appendix J. To determine the benefit of the use of hydrogen in terms of environmental sustainability, an energy equivalent fuel consumption for kerosene (Factor 2.8) is calculated.

$$GWP = \sum_{i=1}^{3} \sum_{j=Taxi_in}^{Taxi_out} m_{ij} \cdot E_i(h)\,\mathrm{d}x \tag{6.17}$$

In Appendix F.2 the difference in GWP of the different propellants is shown. The combustion of hydrogen in this specific mission has approximately 70% less global warming potential than kerosene (not taking into account benefits in SFC through reduction in MTOM by using hydrogen).

6.2.2 Low Noise

A minor target of this challenge is to meet the far-term target for noise reduction. The aim is a stage 4 noise reduction of 42 dB beyond 2035. In the type-certificate data sheet for noise for the B747-400ER the lateral, flyover and approach EPNL are given [75]. The B747-400ER, with a maximum take off weight of 412 t, has a cumulative EPNL of 299.3 dB. So the BWB needs a cumulative EPNL of 257.3dB. This means an average EPNL of 86 dB for every single step (lateral, flyover and approach). A great advantage of this BWB design is that the engines are mounted above the aircraft. This way the engines are shielded from the ground by the aircraft body and shielded from the side by the v-tail. A simulation by the NASA, which is based on real conditions (atmospheric and acoustic), compares the noise emitted by a B777-200 with a BWB [76]. The engine model of the B777 used in the simulation is from the GE90 series. The B777-200 and the BWB are compared concerning their approach noise. The B777-200 has an approach noise of 99.4 dB and the BWB of 83.9 dB. The B747 has an approach noise of 102.3 dB. Only a change in the configuration to a BWB can reduce the noise around 18.4 dB for approach. In appendix Appendix H all BWB configurations of the NASA noise calculation are shown for every single step. In figure Appendix H.1 the noise reduction potential from different BWB designs, which were calculated by NASA, are listed. The main differences between the BWB configuration are the engine pylon position and design, the design of the landing gear and the noise reduction methods of the engine like a chevron nozzle. The main noise component of a BWB is the sideline noise (see figure Appendix H.2). The main sideline noise is emitted by the fan and the jet (see figure Appendix H.3). With the v-tail, which will shield the jet noise, the variable pitch fan (see appendix 3.2) and the BWB configuration a noise reduction of 42 dB is possible.

6.3 Direct Operating Costs

For better comparison to other aircraft types and configurations it is convenient to calculate the direct operating cost per seat mile kilometer (DOC/SMK). A simple DOC-assessment method was developed by J. Thorbeck [77]. The DOC are split into route independent costs and route dependent costs. The route independent costs encompass the capital costs, the insurance costs, personnel maintenance costs and flight crew cost. An important parameter affecting the route independent costs is the operating empty weight. The route dependent costs are based on the fuel costs, the maintenance cost, landing, handling and ATC fees. The fuel costs highly depend on the fuel price. In the technical report "Liquid Hydrogen Fuelled Aircraft – System Analysis" [16] the hydrogen costs range between 0.85 and 1.4 euro per kg. For this DOC calculation a conservative fuel price of 1.4 euro is assumed. In the Appendix Appendix N is the DOC/SMK are shown. The minimum DOC/SMK is located in the design point at 6160 NM. The amount of the DOC/SMK is 0.025 euro which are lower than the DOC for the B747-400ER with 0.03 euro (calculated with the same DOC

method and a fuel price of 0.61 euro per kg). These DOC/SMK do not contain cargo or passenger revenue and a fix fuel price is considered. With the estimated fixed liquid hydrogen price is the BWB better than the B747-400ER.

7 Conclusion

This aircraft design report shows the first iteration of a hydrogen based blended wing body concept. Even though the use of hydrogen as aviation fuel poses many challenges, it is the next logical step to lower aviation impact on environment in times of steadily rising passenger volume. This design promises to be very energy efficient, amounting to a projected 63% reduction in energy consumption compared to the reference aircraft Boeing 747-400ER. Because fuel is a considerable cost factor for an airline, reducing the fuel consumption directly results in lower direct operating costs. Another advantage is the significant decrease by 70% in global warming potential due to hydrogen. Additionally, a noise reduction of 42dB is probable as a result of the BWB configuration, the engine modifications and the tilted stabilizer.

Challenges that need to be addressed are the integration of the aircraft into the existing fleet, modifications to the manufacturing process due to hydrogen and the BWB configuration. Furthermore regulations need to be adapted for the operation with BWB and hydrogen.

There are many opportunities for this aircraft to be a game changer in the aviation industry. The rising political pressure to reduce CO2 emissions even further or raising kerosene prices could lead to an earlier entry into service or additional sales because the aircraft will be profitable faster. The passenger acceptance is a factor that could develop in both negative or positive direction, because some passengers will like the new design, while others will reject the windowless design or consider hydrogen to be too dangerous.

Threats to the concept are the other contenders for an alternative aircraft fuel, lower oil prices or decreased CO_2 regulation.

Appendix

Appendix A Payload Range Diagram

Payload Range Diagram from B747-400ER (PW 4062 Engines)

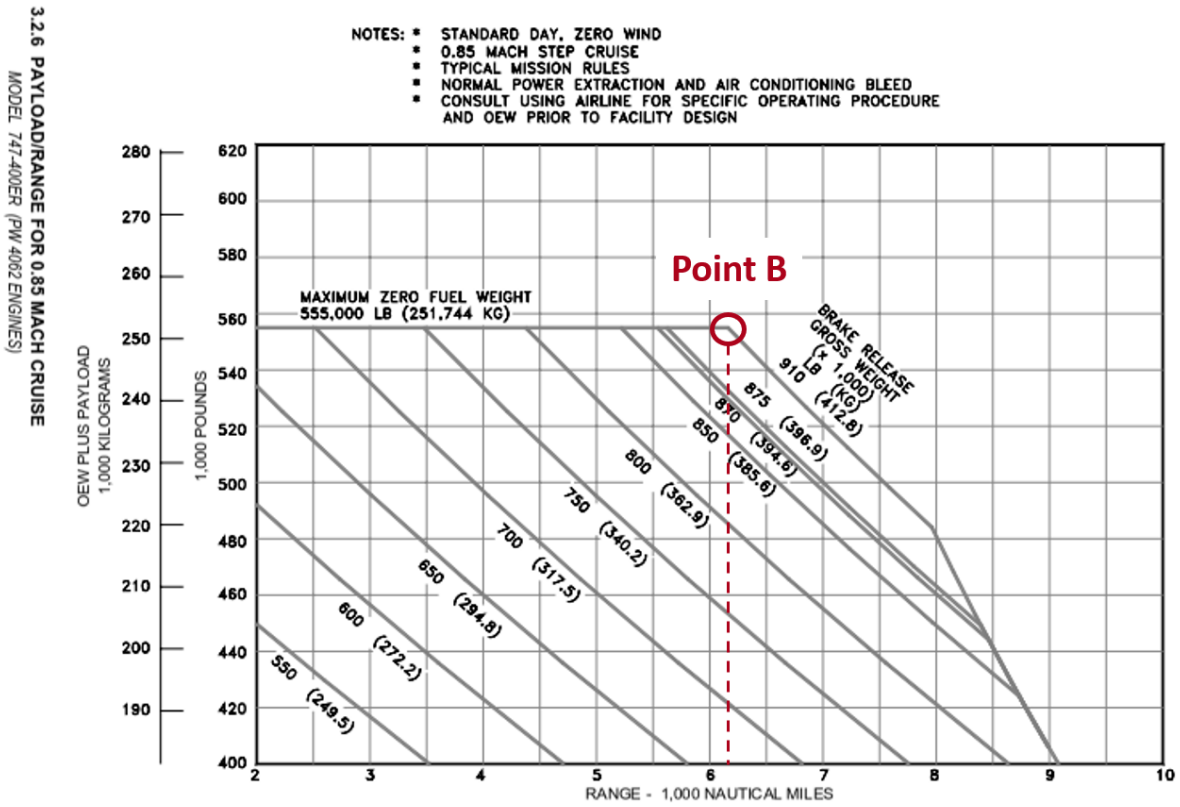

Figure Appendix A.1: Payload Range Diagram

Appendix B Detailed Mass Breakdown

Table Appendix B.1: Detailed mass breakdown Boeing 747-400ER (PW 4062 engines)

Group indication		Mass [kg]	% DEM	% MTOM
Airframe structure	Wing group	49,578	29.6	12.0
	Tail group	6,120	3.7	1.5
	Body group	28,693	17.1	7.0
	Alighting gear group	13,184	7.9	3.2
	Surface controls group	3,679	2.2	0.9
	Engine section or nacelle group	4,078	2.4	1.0
	Group total	105,331	62.9	25.6
Propulsion group	Propulsion Group	23,194	13.8	5.6
	Group total	23,194	13.8	5.6
Airframe services and equipment	Auxiliary Power Unit	465	0.3	0.1
	Instruments, navigational equipment and electronics group	1,948	1.2	0.5
	Hydraulic, pneumatic and electrical group	12,223	7.3	3.0
	Furnishing and equipment group	21,163	12.6	5.1
	Air-conditioning and anti-icing group	2,359	1.4	0.6
	Miscellaneous	837	0.5	0.2
	Group total	38,996	23.3	9.5
Basic empty mass (Delivery empty mass)		**167,534**	**100**	**40.7**
Operational items	Crew provisions	1,027		0.2
	Passenger cabin supplies	4,526		1.1
	Water and toilet chemicals	1,088		0.3
	Safety equipment	1,785		0.4
	Seating	7,875		1.9
	Residual fuel	583		0.1
	Group total	16,301		4.0
Operational empty mass		**183,822**		**44.6**
Payload	Payload	67,177		16.3
	Group total	67,177		16.3
Zero fuel mass		**250,999**		**60.9**
Fuel	Fuel	161,026		39.1
	Group total	161,026		39.1
Maximum takeoff mass		**412,025**		**100**

Table Appendix B.2: Detailed mass breakdown H211

Group indication		Mass [kg]	% DEM	% MTOM
Airframe structure	Wing group	8,569	4.6	2.97
	V-Tail	1,191	0.64	0.41
	Cabin group	71,714	38.50	24.81
	After centerbody	7,982	4.28	2.76
	Alighting gear group	10,161	5.45	3.52
	Surface controls group	2,900	1.56	1.00
	Tank	10,000	5.37	3.46
	Cooling system	2,000	1.07	0.69
	Group total	114,517	61.47	39.62
Propulsion group	Propulsion Group	20,000	10.74	6.92
	Group total	134,517	10.74	6.92
Airframe services	Instruments, navigational equipment and electronics group	3,173	1.7	1.1
and equipment	Hydraulic, pneumatic and electrical group	24,369	13.08	8.43
	Furnishing and equipment group	15,255	8.19	5.29
	Air-conditioning and anti-icing group	6,979	3.75	2..41
	Miscellaneous	1,990	1.07	0.69
	Group total	51.736	27.79	17.92
Basic empty mass (Delivery empty mass)		**186,253**	**100**	**64.45**
Operational items	Crew provisions	934		0.32
	Passenger cabin supplies	4,577		1.58
	Water and toilet chemicals	2,655		0.92
	Safety equipment	1,805		0.62
	Seating	4,779		1.65
	Group total	14,750		5.09
Operational empty mass		**201,003**		**69.55**
Payload	Payload	67,177		23.25
	Group total	67,177		23.25
Zero fuel mass		**268,180**		**92.8**
Fuel	Fuel	20,814		7.20
	Group total	20,814		7.20
Maximum takeoff mass		**288,994**		**100**

Detailed mass breakdown Boeing 747-400ER (PW 4062)

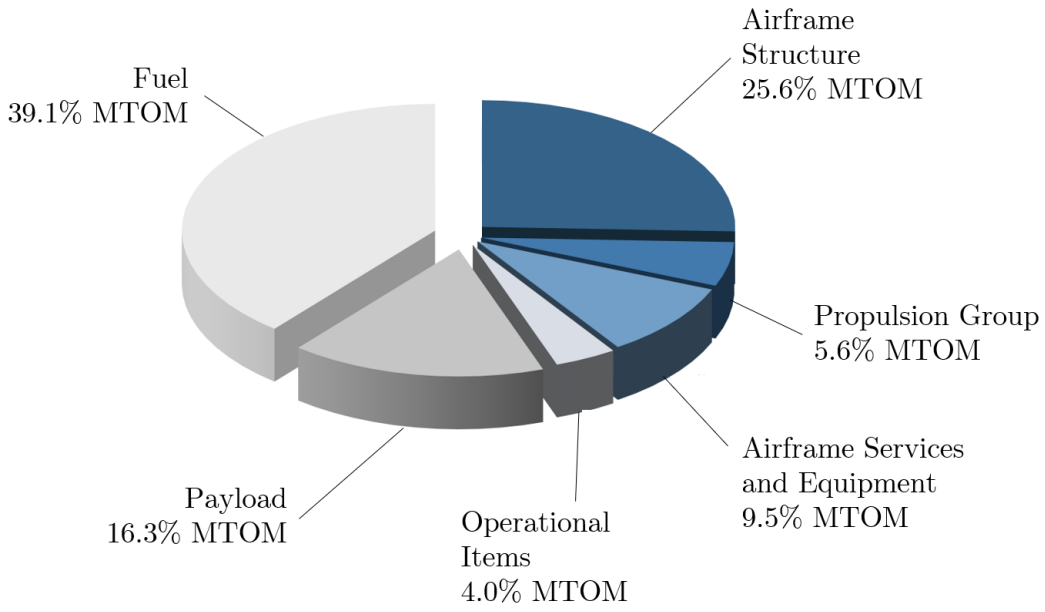

Detailed mass breakdown H211

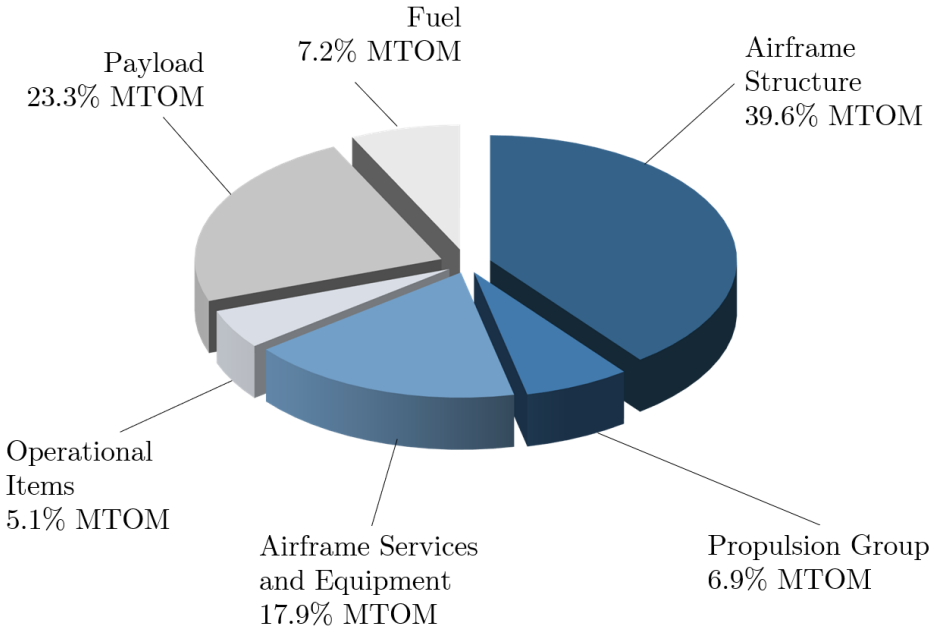

Appendix C Key Technologies

Table Appendix C.1: List of key technologies

Group indication	Concept	Technology	FRB [%]	TRL today
Aircraft configuration	Hybrid-Wing-Body		10-30	4
Aerodynamics	Advanced wingtip device	Blended winglets	3-6	9
	High lift devices	Circulation control wings		
	Hybrid laminar flow		10-15	7
Structural	Composite secondary structures		1	9
Cabin	LED lighting		0.5	9
	Wireless in-flight entertainment		0.5	9
	Lightweight cabin interior		1-5	9
	Windowless design		5-7	4
Systems	APU	Lithium Batteries	1	5
	APU	No APU	1-5	
	Landing Gear	Taxi Bot	1-4	7
	More Electric AC Architecture		1-5	8
New Engine	Geared Turbofan		10-15	7
Architecture	New Engine Core		25-30	2
Advanced Engine Concepts	Fan	Component Improvement	2-6	8
	Fan	Variable Pitch Fan		
	Fan	Very High Bypass Ratio	2-6	7
	Combustor	Micro Mix		
	Compressor	Bling	1-3	3
Nacelle	Buried Engine		1-3	5
Engine Cycles	Boundary Layer Ingestion Inlet		1-3	5
	Ubiquitous Composites		10-15	3
Fuel	Hydrogen		1-3	5

Appendix D Walking Speeds and Waist Sizes

Table Appendix D.1: Walking speeds used in the simulation [78]

Profile	Mean speed [s]	Standard deviation [s]	Maximum speed [s]	Minimum speed [s]
Man	2.45	0.315	3.08	1.82
Woman	2.34	0.344	3.028	1.652
Old Woman	1.77	0.254	2.278	1.262
Old Man	1,93	0.364	2.658	1.202
Mother	2.12	0.275	2.67	1.57

Note: The maximum speeds are calculated by adding twice the standard deviation to the mean value. Similarly, the minimum speeds are obtained by subtracting twice the standard deviation from the mean value.

Table Appendix D.2: Waist sizes used in the simulation [79]

Profile	Mean waist circumference [cm]
Man	31.26
Woman	29.16
Old Woman	31.39
Old Man	33.96
Mother	30.3

Appendix E Insulation Materials

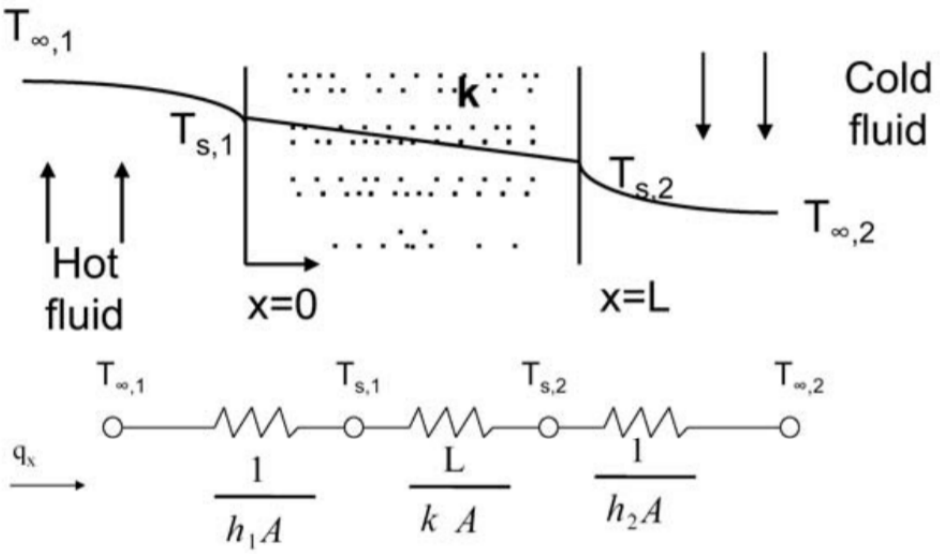

Figure Appendix E.1: Nodal Model of 1D steady state thermal analysis [80]

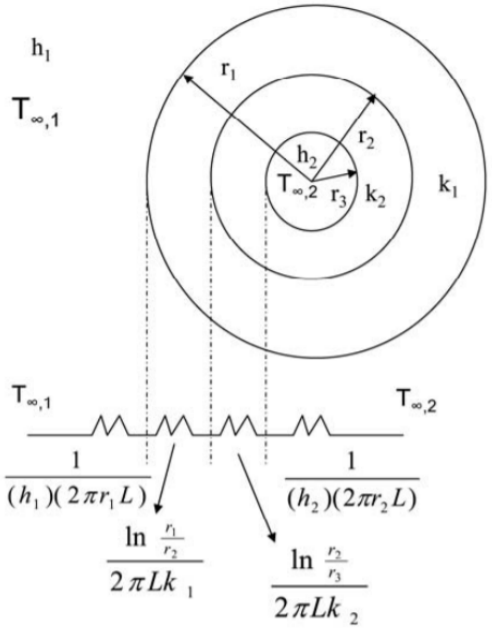

$$q_r = \frac{T_{\infty,2} - T_{\infty,1}}{\sum R_t}$$

Figure Appendix E.2: Schematic Model of 1D steady state thermal analysis [80]

Insulation Material Properties ([41])

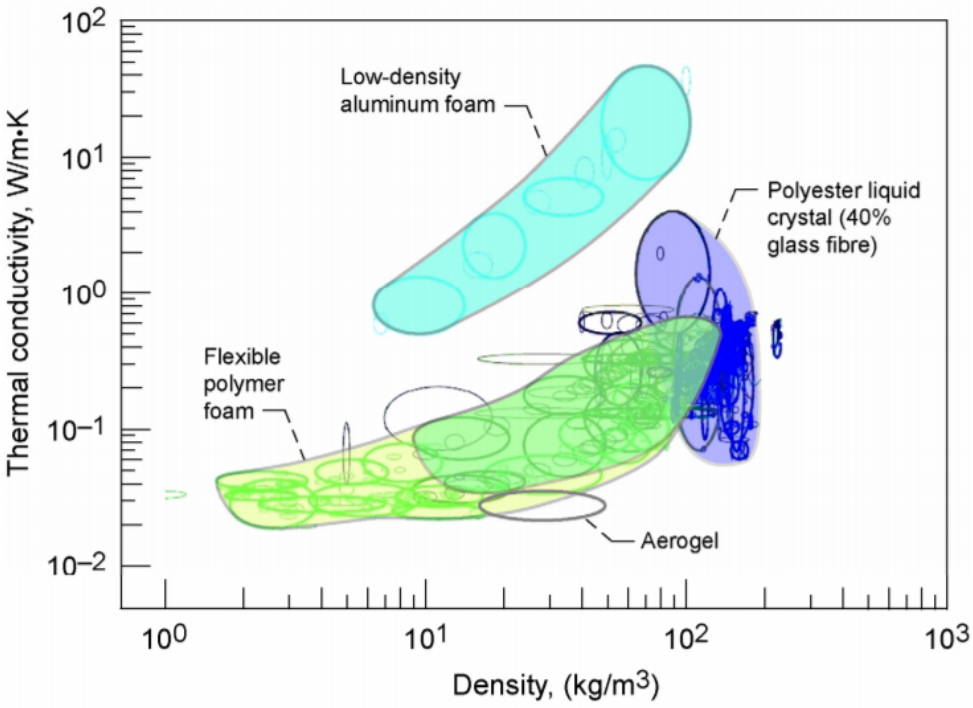

Figure Appendix E.3: Thermal conductivity versus mass density of insulation materials

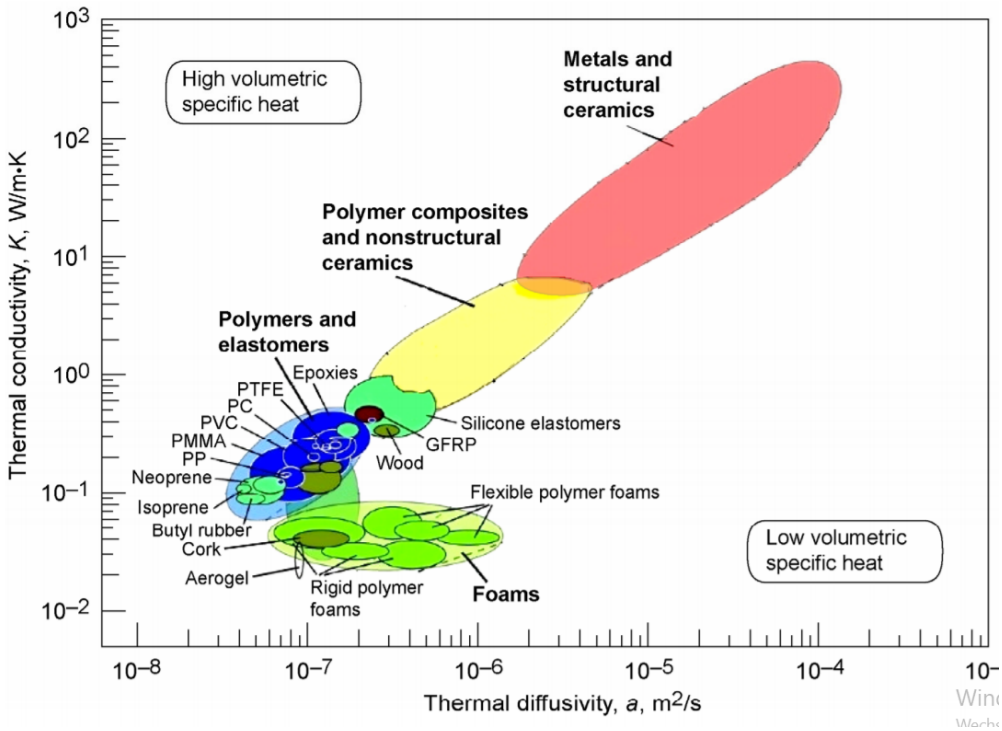

Figure Appendix E.4: Thermal conductivity versus thermal diffusivity

Appendix F Global Warming Potential

Emission Forecast 2035 by EASA in the European Aviation Environmental Report 2016

	2005	2014 *(% change vs. 2005)*	Base forecast 2035 Advanced – Low Technology *(% change vs. 2005)*
Average fuel burn (kg) per passenger kilometre	0.0388	0.0314 *(-19%)*	0.0209 – 0.0222 *(-46%) (-43%)*
CO_2 (Mt)	144	151 *(+5%)*	207 – 219 *(+44%) (+53%)*
NO_x (1,000 t)	650	732 *(+13%)*	920 – 1049 *(+42%) (+61%)*
NO_x below 3,000 feet (1,000 t)	53.3	58.8 *(+10%)*	73.3 – 83.1 *(+37%) (+56%)*
HC (1,000 t)	20.8	17.0 *(-18%)*	22.9 *(+10%)*
HC below 3,000 feet (1,000 t)	7.8	6.4 *(-18%)*	11.0 *(+40%)*
CO (1,000 t)	143	133 *(-7%)*	206 *(+44%)*
CO below 3,000 feet (1,000 t)	52.4	48.2 *(-8%)*	85.5 *(+63%)*
volatile PM (1,000 t)	4.18	4.47 *(+7%)*	6.93 *(+66%)*
volatile PM below 3,000 feet (1,000 t)	0.27	0.27 *(-1%)*	0.41 *(+50%)*
non-volatile PM (1,000 t)	2.67	2.38 *(-11%)*	3.16 *(+18%)*
non-volatile PM below 3,000 feet (1,000 t)	0.15	0.13 *(-14%)*	0.17 *(+11%)*

Figure Appendix F.1: Summary of emission indicators based on IMPACT data

Table Appendix F.1: Global Warming Potentials of Carbon Dioxide, Water Vapor and Nitrogen Oxides over Altitude [73]

Altitude (km)	E_{CO_2}	E_{H_2O}	E_{NO_x}
0	1	0	-7.1
1	1	0	-7.1
2	1	0	-7.1
3	1	0	-4.3
4	1	0	-1.5
5	1	0	6.5
6	1	0	14.5
7	1	0	37.5
8	1	0	60.5
9	1	0	64.7
10	1	0.24	68.9
11	1	0.34	57.7
12	1	0.43	46.5
13	1	0.53	25.6
14	1	0.62	4.6
15	1	0.72	0.6

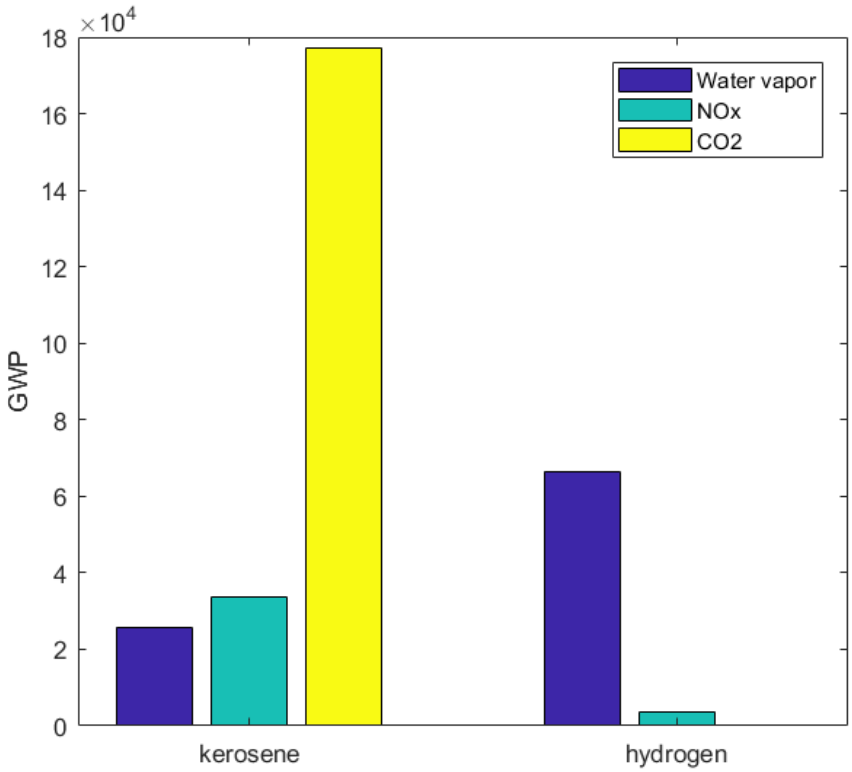

Figure Appendix F.2: Global Warming Potential of kerosene versus hydrogen

Appendix G Propulsion System

The following figure displays the main components of the VPF, which can be integrated into the center-body of current turbofan engines. Simultaneous blade pitch variation is executed by the rotary actuator and the variable pitch assembly consisting of a collector ring with attached pitch arms. [81]

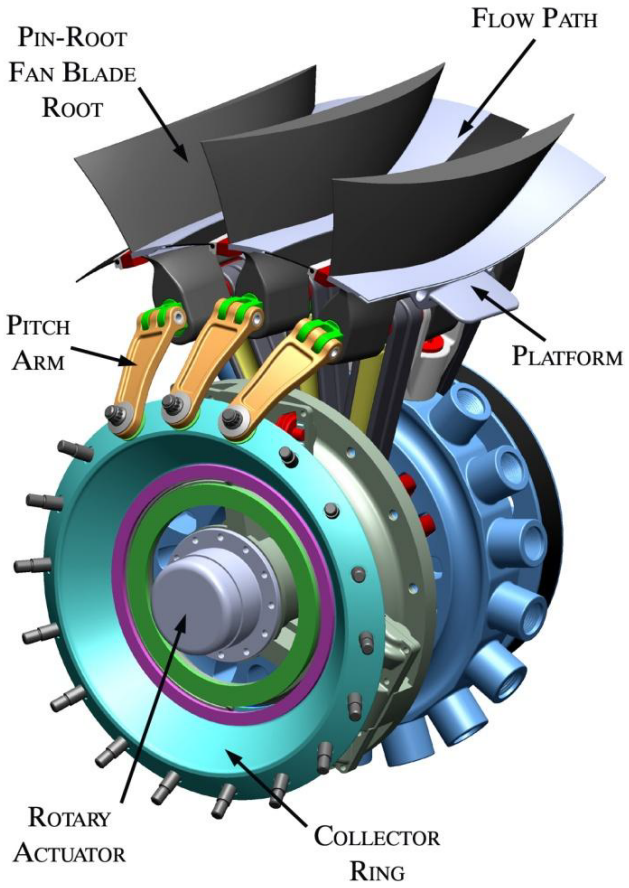

Figure Appendix G.1: Variable pitch mechanism [81]

Table Appendix G.1: Engine parameters for cruise

Parameter	Unit	PW4062	GVPTF
μ	[-]	4.6	12
TET	[K]	1700	1800
OPR	[-]	31	50
η_{Fan}	[-]	0.9	0.92
$\eta_{Compressor}$	[-]	0.88	0.9
$\eta_{Turbine}$	[-]	0.89	0.9
$\eta_{Throttle}$	[-]	0.96	0.98
SFC	[kg/daNh]	0.6549	0.1995

Appendix H Noise

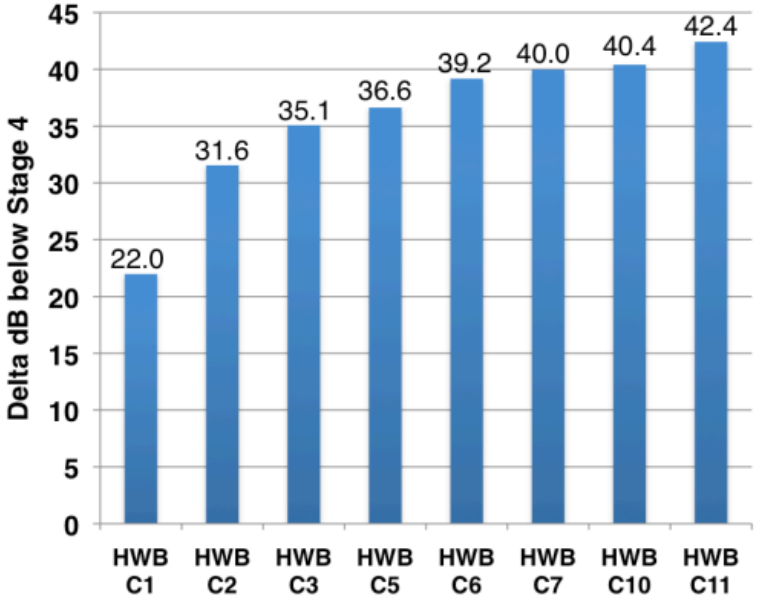

Figure Appendix H.1: Cumulative aircraft system noise levels relative to the stage 4 level of HWB aircraft and technology options studied[82]

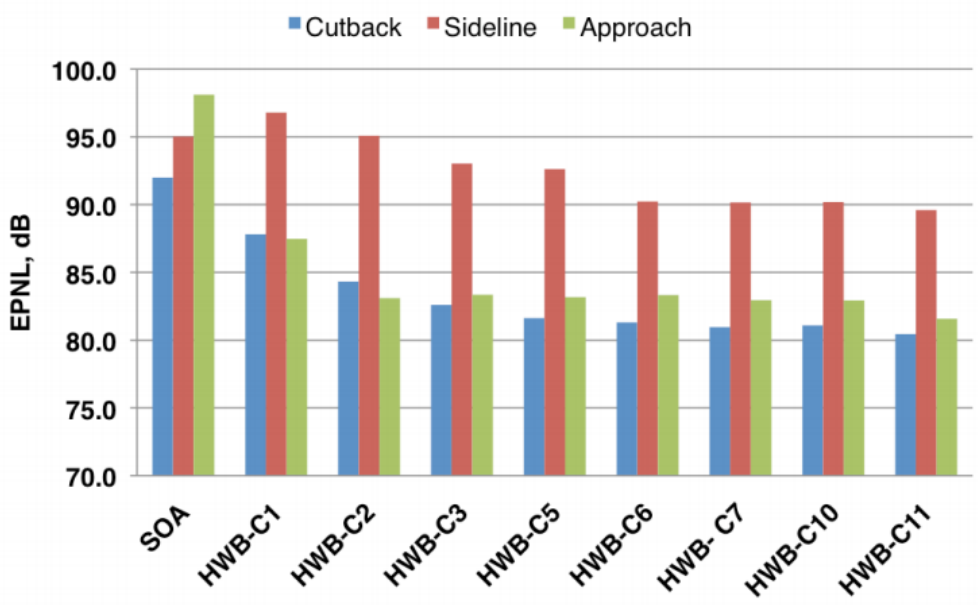

Figure Appendix H.2: Predicted EPNL for the Boeing 777-like aircraft and different configurations of the HWB [82]

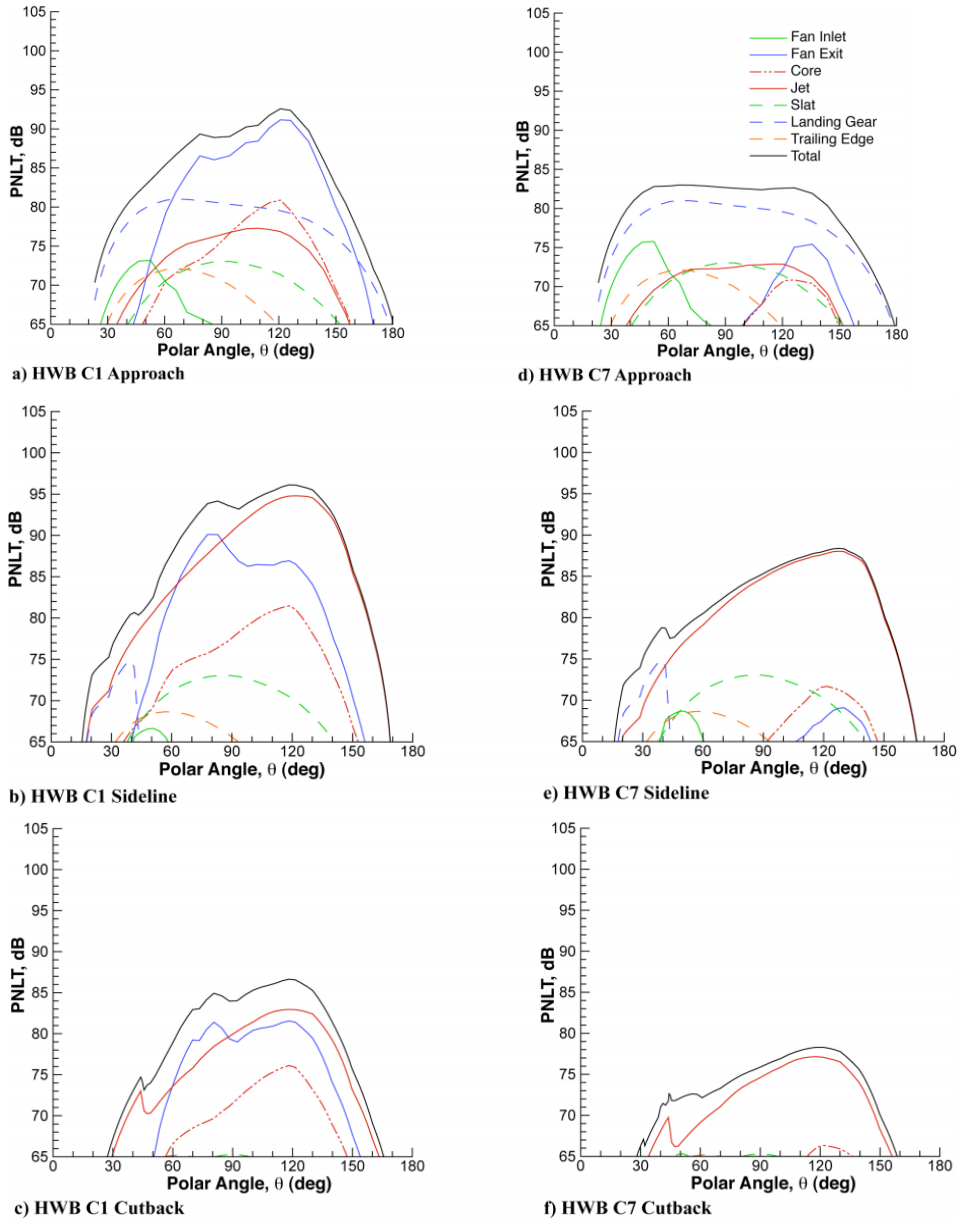

Figure Appendix H.3: Tone-corrected perceived noise level, PNLT, as a function of flyover angle (observer at 90 degrees) at approach, sideline and cutback conditions for Configuration 1 (a, b, and c) and 7 (d, e, and f) [82]

Appendix I Control Surfaces

Table Appendix I.1: V-Tail parameters

Parameter	Arithmetic middle values	Stabilizer data
Tail to wing area ratio	0.066	0.066
Aspect ratio	1.855	1.855
Tapper ratio	0.3723	0.3723
V-tail area [m^2]	-	86.63
Span of one tail [m]	-	8.9
V-tail angle [°]	-	80

Appendix J Mission Characteristics

Engine Start and Warm up			
		B747	H211
Parameters	**Unit**	**Value**	**Value**
Height	[m]	-	0.000
Velocity	[m/s]	-	0.000
Range	[m]	-	0.000
Time	[s]	-	720.000
RFFF	[-]	0.996	0.996
MFFF	[-]	-	0.999
BFFF	[-]	-	-
IFFF	[-]	-	0.999
Mass Start	[kg]	415,786.520	289,277.568
Mass End	[kg]	414,130.000	289,025.394
Mass Delta	[kg]	1,656.520	252.174
Energy Consumption	[J]	70,402,100,000.001	30,260,862,322.147

Taxi			
		B747	H211
Parameters	**Unit**	**Value**	**Value**
Height	[m]	-	0.000
Velocity	[m/s]	-	12.861
Range	[m]	-	5,401.662
Time	[s]	-	420.000
RFFF	[-]	0.997	0.995
MFFF	[-]	-	0.998
BFFF	[-]	-	-
TFFF	[-]	-	0.998
Mass Start	[kg]	414,130.000	289,025.394
Mass End	[kg]	412,770.000	289,025.394
Mass Delta	[kg]	1,360.000	0.000
Energy Consumption	[J]	57,800,000,000.000	58,347,001,371.647

Take Off			
		B747	H211
Parameters	**Unit**	**Value**	**Value**
Height	[m]	-	5.334
Velocity	[m/s]	-	69.991
Range	[m]	-	3,322.000
Time	[s]	-	47.463
RFFF	[-]	0.995	0.995
MFFF	[-]	-	0.998
BFFF	[-]	-	-
IFFF	[-]	-	0.999
Mass Start	[kg]	412,770.000	289,025.394
Mass End	[kg]	410,706.150	288,710.420
Mass Delta	[kg]	2,063.850	314.974
Energy Consumption	[J]	87,713,624,999.999	37,796,825,841.183

Figure Appendix J.1

Climb			
		B747	H211
Parameters	**Unit**	**Value**	**Value**
Height	[m]	-	7,466.667
Velocity	[m/s]	-	175.845
Range	[m]	-	369,699.883
Time	[s]	-	2,102.414
RFFF	[-]	0.984	-
MFFF	[-]	-	-
BFFF	[-]	-	0.994
IFFF	[-]	-	0.996
Mass Start	[kg]	410,706.150	288,710.420
Mass End	[kg]	404,030.830	287,680.166
Mass Delta	[kg]	6,675.320	1,030.254
Energy Consumption	[J]	283,701,096,957.821	123,630,463,357.915
Cruise			
		B747	**H211**
Parameters	**Unit**	**Value**	**Value**
Height	[m]	-	11,200.000
Velocity	[m/s]	-	263.768
Range	[m]	-	10,760,180.979
Time	[s]	-	40,794.083
RFFF	[-]	0.668	-
MFFF	[-]	-	-
BFFF	[-]	-	0.904
IFFF	[-]	-	0.941
Mass Start	[kg]	404,030.830	287,680.166
Mass End	[kg]	269,879.801	270,665.865
Mass Delta	[kg]	134,151.029	17,014.301
Energy Consumption	[J]	5,701,418,719,041.550	2,041,716,179,813.940
Descent			
		B747	**H211**
Parameters	**Unit**	**Value**	**Value**
Height	[m]	-	7,907.941
Velocity	[m/s]	-	167.206
Range	[m]	-	278,439.138
Time	[s]	-	1,665.246
RFFF	[-]	0.999	0.999
MFFF	[-]	-	1.000
BFFF	[-]	-	-
IFFF	[-]	-	1.000
Mass Start	[kg]	269,879.801	270,665.865
Mass End	[kg]	269,609.922	270,607.062
Mass Delta	[kg]	269.880	58.803
Energy Consumption	[J]	11,469,891,559.001	7,056,317,816.600

Figure Appendix J.2

Landing, Taxi & Shutdown			
		B747	H211
Parameters	**Unit**	**Value**	**Value**
Height	[m]	-	0.000
Velocity	[m/s]	-	12.861
Range	[m]	-	5,401.662
Time	[s]	-	420.000
RFFF	[-]	0.999	0.995
MFFF	[-]	-	0.998
BFFF	[-]	-	-
TFFF	[-]	-	0.998
Mass Start	[kg]	269,879.801	270,607.062
Mass End	[kg]	269,609.922	270,607.062
Mass Delta	[kg]	269.880	0.000
Energy Consumption	[J]	11,469,891,559.001	54,628,800,688.593

Climb Alternate			
		B747	H211
Parameters	**Unit**	**Value**	**Value**
Height	[m]	-	3,733.333
Velocity	[m/s]	-	184.535
Range	[m]	-	72,997.233
Time	[s]	-	395.574
RFFF	[-]	0.997	-
MFFF	[-]	-	-
BFFF	[-]	-	0.999
IFFF	[-]	-	0.999
Mass Start	[kg]	269,609.922	270,607.062
Mass End	[kg]	268,787.362	270,424.942
Mass Delta	[kg]	822.560	182.120
Energy Consumption	[J]	34,958,802,959.890	21,854,442,186.069

Cruise Alternate			
		B747	H211
Parameters	**Unit**	**Value**	**Value**
Height	[m]	-	5,600.000
Velocity	[m/s]	-	180.243
Range	[m]	-	130,343.905
Time	[s]	-	723.158
RFFF	[-]	0.994	-
MFFF	[-]	-	-
BFFF	[-]	-	0.999
IFFF	[-]	-	0.999
Mass Start	[kg]	268,787.362	270,424.942
Mass End	[kg]	267,224.263	270,217.686
Mass Delta	[kg]	1,563.098	207.256
Energy Consumption	[J]	66,431,679,935.774	120,000,000.000

Figure Appendix J.3

Descend to Holding			
		B747	H211
Parameters	**Unit**	**Value**	**Value**
Height	[m]	-	3,806.650
Velocity	[m/s]	-	122.912
Range	[m]	-	140,756.488
Time	[s]	-	1,145.180
RFFF	[-]	0.999	0.999
MFFF	[-]	-	1.000
BFFF	[-]	-	-
IFFF	[-]	-	1.000
Mass Start	[kg]	267,224.263	270,217.686
Mass End	[kg]	266,957.039	270,158.981
Mass Delta	[kg]	267.224	58.705
Energy Consumption	[J]	11,357,031,184.546	7,044,633,693.108

Holding			
		B747	H211
Parameters	**Unit**	**Value**	**Value**
Height	[m]	-	457.200
Velocity	[m/s]	-	128.611
Range	[m]	-	231,499.800
Time	[s]	-	1,800.000
RFFF	[-]	0.983	
MFFF	[-]	-	
BFFF	[-]	-	0.996
IFFF	[-]	-	0.997
Mass Start	[kg]	266,957.039	270,158.981
Mass End	[kg]	262,483.300	269,455.483
Mass Delta	[kg]	4,473.739	703.498
Energy Consumption	[J]	190,133,905,952.387	84,419,765,466.135

Descend Alternate			
		B747	H211
Parameters	**Unit**	**Value**	**Value**
Height	[m]	-	304.800
Velocity	[m/s]	-	85.889
Range	[m]	-	26,302.374
Time	[s]	-	306.235
RFFF	[-]	0.999	1.000
MFFF	[-]	-	0.999
BFFF	[-]	-	-
IFFF	[-]	-	1.000
Mass Start	[kg]	262,483.300	269,455.483
Mass End	[kg]	262,220.817	269,396.943
Mass Delta	[kg]	262.483	58.540
Energy Consumption	[J]	11,155,540,247.408	7,024,762,887.040

Figure Appendix J.4

Landing, Taxi & Shutdown			
		B747	H211
Parameters	**Unit**	**Value**	**Value**
Height	m	-	0.000
Velocity	m/s	-	12.861
Range	m	-	5,401.662
Time	s	-	420.000
RFFF	-	0.999	0.995
MFFF	-	-	0.998
BFFF	-	-	-
IFFF\TFFF	-	-	0.998
Mass Start	kg	262,220.817	269,396.943
Mass End	kg	261,958.596	269,396.943
Mass Delta	kg	262.221	0.000
Energy Consumption	J	11,144,384,707.162	-

Figure Appendix J.5

Appendix K Airport Infrastructure

Figure Appendix K.1: Airport and Fuel Station Concept by Total [83]

Appendix L CAD

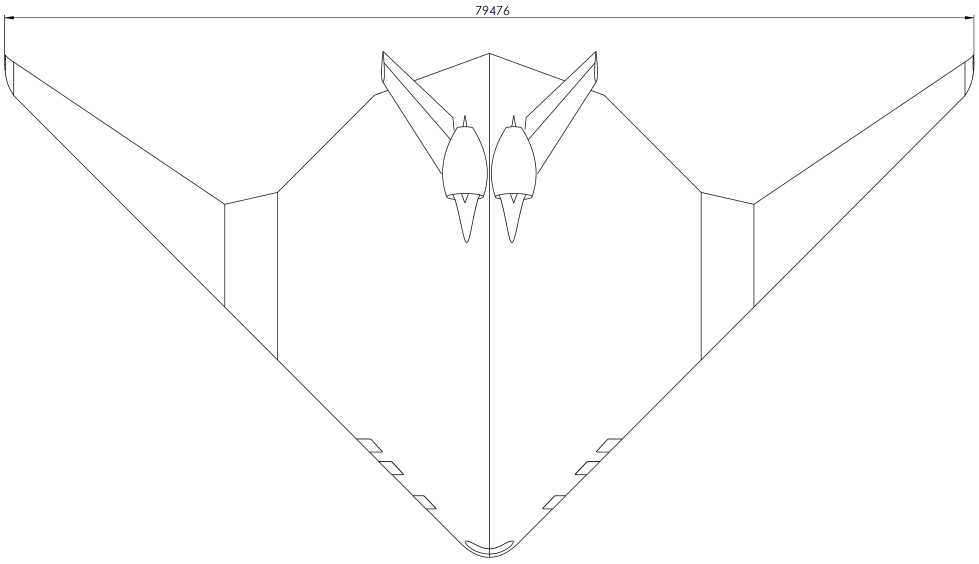

Figure Appendix L.1: Topview

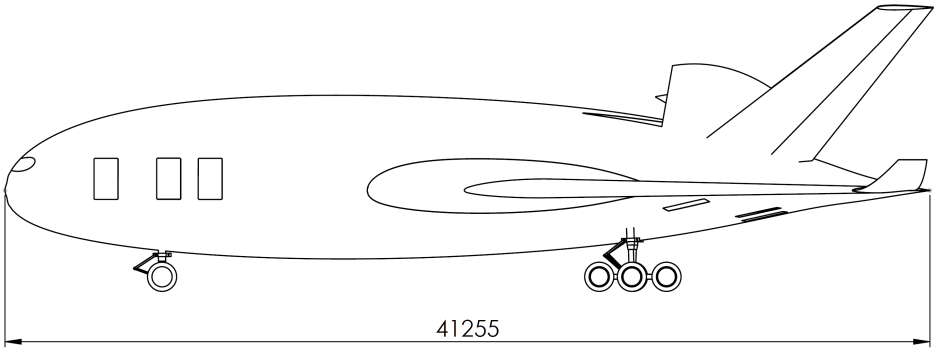

Figure Appendix L.2: Sideview

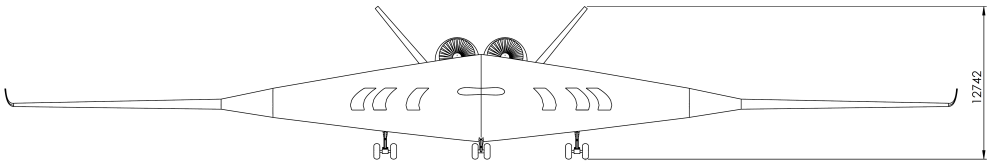

Figure Appendix L.3: Frontview

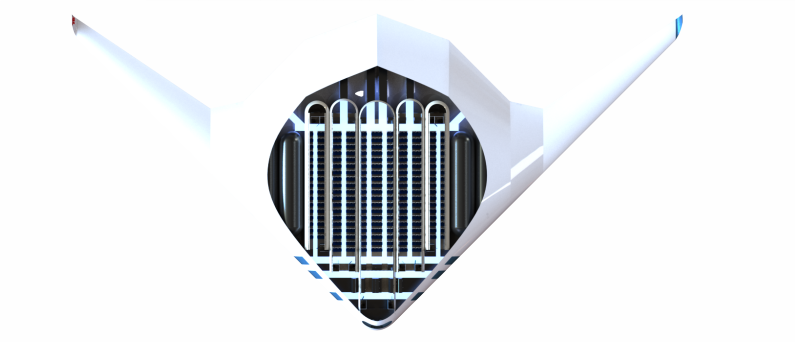

Figure Appendix L.4: Top view cabin layout

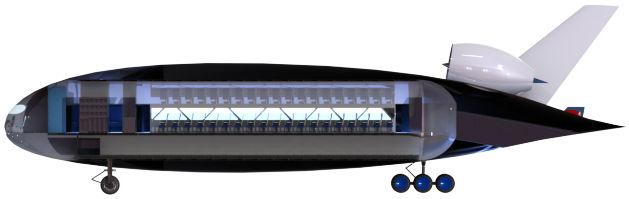

Figure Appendix L.5: Side view cabin

Appendix M Passenger Load

- "At least 40% of the passenger load must be female.
- At least 35% of the passenger load must be over 50 years of age.
- At least 15% of the passenger load must be female and over 50 years of age.
- Three life-size dolls, not included as part of the total passenger load, must be carried by passengers to simulate live infants 2 years old and younger." [52]

Appendix N DOC

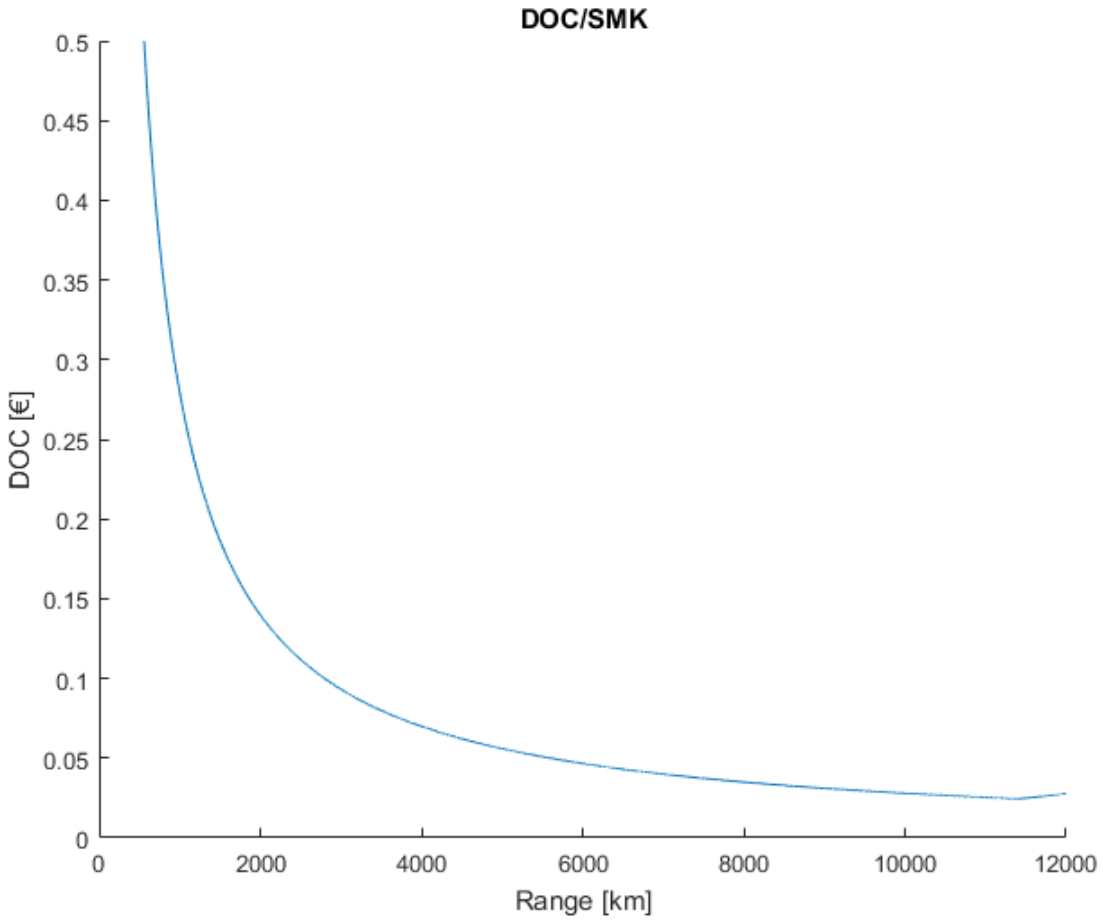

Figure Appendix N.1: Direct Operating Cost

Appendix O Performance

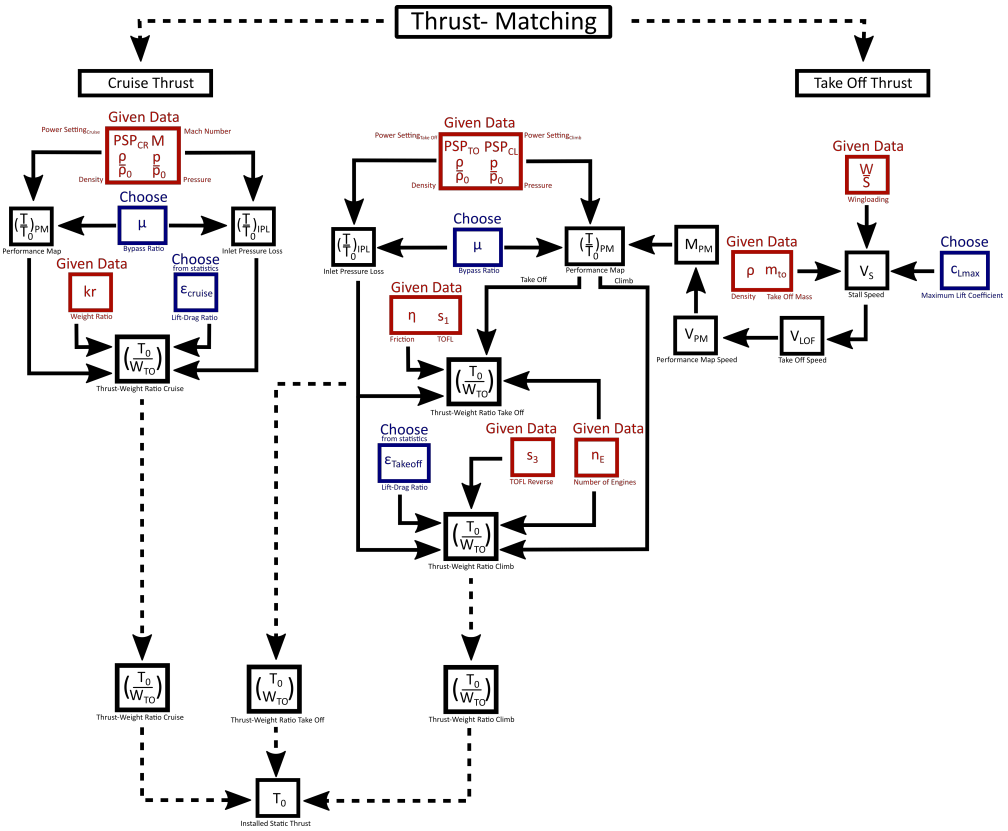

Figure Appendix O.1: Thrustmatching

References

[1] Werner Kolhoff. *Ölquellen sprudeln immer weniger*. URL: https://www.lr-online.de/nachrichten/wirtschaft/oelquellen-sprudeln-immer-weniger%5C_aid-4632448. (accessed: 08.06.2018).

[2] NASA's Jet Propulsion Laboratory. *Graphic: The relentless rise of carbon dioxide*. URL: https://climate.nasa.gov/climate%5C_resources/24/graphic-the-relentless-rise-of-carbon-dioxide/. (accessed: 16.06.2018).

[3] K.M. Schure J.G.J. Olivier and J.A.H.W. Peters. *Trends in Global CO2 and Total grennhouse Gas Emissions*. PBL Netherlands Environmentall Assessment Agency, 2017.

[4] Dilino. *Daily carbon dioxide (CO2) emissions on earth*. URL: http://environment.dilino.org/co2/emission.de.html. (accessed: 14.06.2018).

[5] IATA. *Fact Sheet Climate Change and CORSIA*. URL: http://www.iata.org/pressroom/facts%5C_figures/fact%5C_sheets/Documents/fact-sheet-climate-change.pdf. (accessed: 17.06.2018).

[6] BDL – Bundesverband der Deutschen Luftverkehrswirtschaft e. V. *Klimaschutzreport 2017*. URL: https://www.bdl.aero/download/2681/klimaschutz-report%5C_2017%5C_v5.pdf. (accessed: 15.06.2018).

[7] AIRBUS S.A.S. *Global Market Forecast - Growing Horizons 2017-2036*. AIRBUS, 2017.

[8] European Commission. *Flightpath 2050 - Europe's Vision for Aviation*. URL: https://ec.europa.eu/transport/sites/transport/files/modes/air/doc/flightpath2050.pdf. (accessed: 18.06.2018).

[9] United Nations. *Paris Agreement*. URL: https://unfccc.int/sites/default/files/english%5C_paris%5C_agreement.pdf. (accessed: 25.06.2018).

[10] IATA. *Technology Roadmap*. IATA, 2013.

[11] Boeing Commercial Airplanes. *Current Market Outlook Airplanes 2016-2035*. Boeing, 2016.

[12] Andrew Gordon. *Global Market Forecast - Drivers and Results*. URL: https://www.airbus.com/content/dam/corporate-topics/financial-and-company-information/Global-Market-Forecast-presentation-Andrew-Gordon-Redburn.pdf. (accessed: 26.06.2018).

[13] Deutsche Lufthansa AG. *Sustainability Report 2018*. URL: https://www.lufthansagroup.com/fileadmin/downloads/en/responsibility/balance-2018-epaper/%5C#44. (accessed: 14.06.2018).

[14] International Transport Forum. *ITF Transport Outlook 2017*. 2017, p. 224. DOI: https://doi.org/https://doi.org/10.1787/9789282108000-en. URL: https://www.oecd-ilibrary.org/content/publication/9789282108000-en.

[15] R. Singh F. haglind A. Hasselrot. "Potential of reducing the environmental impact of aviation by using hydrogen Part I: Background, prospects and challenges". In: *The Aeronautical Journal* (Sept. 2006).

[16] Airbus Deutschland GmbH. *Liquid Hydrogen Fuelled Aircraft - System Analysis*. URL: http://www.fzt.haw-hamburg.de/pers/Scholz/dglr/hh/text%5C_2004%5C_02%5C_26%5C_Cryoplane.pdf. (accessed: 26.06.2018).

[17] Boeing Commercial Airplanes. *747-400 Airplane Characteristics for Airport Planning*. URL: https://www.boeing.com/resources/boeingdotcom/commercial/airports/acaps/747_4.pdf. (accessed: 30.06.2018).

[18] R. H. Liebeck. "Design of the BlendedWing Body Subsonic Transport". In: *Journal of Aircraft* 41.7 (2004), pp. 1–16. ISSN: 0021-8669. DOI: https://arc.aiaa.org/doi/10.2514/1.9084.

[19] R.W. Derksen and Tim Rogalsky. “Bezier-PARSEC: An optimized aerofoil parameterization for design”. In: *Advances in Engineering Software* 41.7 (2010). Advances in Structural Optimization, pp. 923–930. ISSN: 0965-9978. DOI: https://doi.org/10.1016/j.advengsoft.2010.05.002. URL: http://www.sciencedirect.com/science/article/pii/S0965997810000529.

[20] Martin Hepperle. *MH 49*. URL: https://www.mh-aerotools.de/airfoils/mh49koo.htm.

[21] Rober Luckner. *Flugmechnaik 2 (Flugdynamik)*. TU Berlin, 2016.

[22] OpenCFD. *Standard solvers*. URL: https://www.openfoam.com/documentation/user-guide/standard-solvers.php.

[23] Daniel Reckzeh. “Der intelligente Tragflügel”. In: *DGLR - Luft- und Raumfahrt* (Jan. 2018).

[24] Grönstedt et al. *Ultra Low Emission Technology Innovations for mid-century aircraft turbine engines*. URL: http://publications.lib.chalmers.se/records/fulltext/237482/local%5C_237482.pdf. (accessed: 29.06.2018).

[25] Deutsches Zentrum für Luft- und Raumfahrt e. V. *Neue Triebwerke: stark, leise und sauber*. URL: https://www.dlr.de/next/desktopdefault.aspx/tabid-6627/10886%5C_read-24695/. (accessed: 29.06.2018).

[26] Rolls-Royce. *The Jet Engine*. Wiley, 2005. ISBN: 9781119065999.

[27] A. H. LEFEBVRE. “Fuel effects on gas turbine combustion-liner temperature, pattern factor, and pollutant emissions”. In: *Journal of Aircraft* 21.11 (Nov. 1984), pp. 887–898. DOI: 10.2514/3.45059. URL: https://doi.org/10.2514/3.45059.

[28] S. Boerner et al. “Development and integration of a scalable low NOx combustion chamber for a hydrogen-fueled aerogas turbine”. In: *Progress in Propulsion Physics*. EDP Sciences, 2013. DOI: 10.1051/eucass/201304357. URL: https://doi.org/10.1051/eucass/201304357.

[29] Willy J. G. Bräunling. *Flugzeugtriebwerke: Grundlagen, Aero-Thermodynamik, Ideale und reale Kreisprozesse, Thermische Turbomaschinen, Komponenten, Emissionen und Systeme*. Springer Vieweg, 2015. ISBN: 9783642345388.

[30] Andreas Petrusson. *Aerodynamic Evaluation of Nacelles for Engines with Ultra High Bypass Ratio*. URL: http://publications.lib.chalmers.se/records/fulltext/247917/247917.pdf. (accessed: 29.06.2018).

[31] MTU Aero Engines. *Geared turbofan - engine of the future*. URL: http://www.mtu.de/fileadmin/EN/7%5C_News%5C_Media/1%5C_Press/3%5C_Press%5C_kits/Singapore%5C_Air%5C_Show%5C_2016/Backgrounder%5C_GTF%5C_ENG.pdf. (accessed: 29.06.2018).

[32] Pratt& Whitney. *Pratt & Whitney GTF Engines Power*. URL: http://www.purepowerengine.com/puresolution.htm. (accessed: 29.06.2018).

[33] Paul Fletcher Philip P. Walsh. *Gas turbine performance*. Blackwell Science Ltd (Black Publishing Company, 2004. ISBN: 9783446423411.

[34] Jiri Dehmel. *Bewertung und Analyse des Entwicklungsstands variabler Rotorschaufeln in Gasturbinen*. Sept. 2017.

[35] Robert S. Mazzawy. *Performance Study for Benefits of Variable Pitch Composite Fan*. June 2010.

[36] Christopher Hughes. *Boundary Layer Ingestion Propulsion*. URL: https://www1.grc.nasa.gov/aeronautics/bli/. (accessed: 29.06.2018).

[37] Wilfert et al. *New Environmental Friendly Aero Engine Core Concepts*. URL: http://citeseerx.ist.psu.edu/viewdoc/download?doi=10.1.1.619.6911&rep=rep1&type=pdf. (accessed: 29.06.2018).

[38] Dries Verstraete. *The Potential of Liquid Hydrogen for long range aircraft propulsion*. 2009. URL: https://core.ac.uk/download/pdf/139335.pdf.

[39] U.S. Secretary of Commerce on behalf of the United States of America. *NIST Chemistry WebBook, SRD 69*. 2017. URL: https://webbook.nist.gov/chemistry/fluid/.

[40] Christopher Winnefeld et al. *Modelling and Designing Cryogenic Hydrogen Tanks for Future Aircraft Applications*. 2018. URL: www.mdpi.com/1996-1073/11/1/105/pdf.

[41] Subodh K. Mital et al. *Review of Current State of the Art and Key Design Issues With Potential Solutions for Liquid Hydrogen Cryogenic Storage Tank Structures for Aircraft Applications*. 2006. URL: https://ntrs.nasa.gov/archive/nasa/casi.ntrs.nasa.gov/20060056194.pdf.

[42] Prof. Ronak Shah Patel PratikKumar BaldevBhai. *Design and Optimization of Cryogenic Storage Vessel*. 2014. URL: https://www.ijedr.org/papers/IJEDR1501040.pdf.

[43] Phani Raj. "Principles of heat transfer, 3rd edit., Frank Kreith, Intext Educational Publishers, New York (1973). 656 pages". In: *AIChE Journal* 20.2 (Mar. 1974), pp. 415–415. DOI: 10.1002/aic.690200244. URL: https://doi.org/10.1002/aic.690200244.

[44] Sandra K. S. Boetcher. *Natural Convection from Circular Cylinders (SpringerBriefs in Applied Sciences and Technology)*. Springer, 2014. ISBN: 978-3-319-08132-8. URL: https://www.amazon.com/Convection-Circular-Cylinders-SpringerBriefs-Technology-ebook/dp/B00S16UZ1E?SubscriptionId=0JYN1NVW651KCA56C102%5C&tag=techkie-20%5C&linkCode=xm2%5C&camp=2025%5C&creative=165953%5C&creativeASIN=B00S16UZ1E.

[45] Gulru Babac, Altug Sisman, and Tolga Cimen. "Two-dimensional thermal analysis of liquid hydrogen tank insulation". In: *International Journal of Hydrogen Energy* 34.15 (Sept. 2009), pp. 6357–6363. DOI: 10.1016/j.ijhydene.2009.05.052. URL: https://doi.org/10.1016/j.ijhydene.2009.05.052.

[46] M. et. al. Schmidt. *Contributions of Cabin Related and Ground Operation Technologies Towards Flightpath 2050*. Sept. 2013.

[47] I. Wetzel and A. Hildebrand. *Realitätsnah und forschungseffizient: Die Akzeptanzmessung zukünftiger Kabinenkonzepte im digitalen Mock-Up*. Sept. 2013.

[48] FlightGlobal. *A different class*. URL: https://www.flightglobal.com/sponsored/airbus/interiors/. (accessed: 25.06.2018).

[49] S. et. al. Bagassi. *Aircraft Preliminary Design: A windowless concept*. Jan. 2015.

[50] Achim Leder (auth.) *Komfortgewinn für Passagiere auf Langstreckenflügen: Validierung chronobiologisch wirksamer Kabinenbeleuchtung zur Jetlag-Reduktion*. 1st ed. Gabler Verlag, 2016. ISBN: 978-3-658-14168-4. URL: http://gen.lib.rus.ec/book/index.php?md5=68eafe14ec2caa1da1cc38e

[51] Lufthansa Cargo AG. *Pallets, containers and fleet*. URL: https://lufthansa-cargo.com/documents/20184/27422/lhc13026%5C_lademittelbroschuere%5C_20140402%5C_nicht%5C_druckbar.pdf/65d54532-5bcc-4315-9e0f-4840cb239953. (accessed: 29.06.2018).

[52] European Aviation Safety Agency. *Certicifation Specifications and Acceptable Means of Compliance for Large Aeroplanes - CS-25*. European Aviation Safety Agency, 2016.

[53] M. Berens N. Dzikus. *Numerische Simulation der Passagierevakuierung aus Wide-Body Flugzeugen mit Lower Deck Seating Compartments*. June 2005.

[54] M. Hepperle R. Sturm. *Crashworthiness and ditching behaviour of blended-wing-body (BWB) aircraft design*. June 2015.

[55] J. Roskam. *Airplane Design*. DARcorporation, 1985. ISBN: 9781884885556.

[56] Egbert Torenbeek. *Synthesis of Subsonic Airplane Design*. Kluwer Academic Publishers, 1982. ISBN: 9789024727247.

[57] Kevin R. Bradley. *A Sizing Methodology for the Conceptual Design of Blended-Wing-Body Transports*. URL: https://ntrs.nasa.gov/archive/nasa/casi.ntrs.nasa.gov/20040110949.pdf. (accessed: 01.07.2018).

[58] Prof. Dr.-Ing. Dieter Scholz. *Die Blended Wing Body(BWB) Flugzeugkonfiguration.* URL: http://www.haw-hamburg.de/pers/Scholz/dglr/hh/text%5C_2006%5C_09%5C_28%5C_BWB.pdf. (accessed: 30.06.2018).

[59] R. Liebeck, M. Page, and B. Rawdon. "Blended-wing-body subsonic commercial transport". In: *36th AIAA Aerospace Sciences Meeting and Exhibit.* American Institute of Aeronautics and Astronautics, Jan. 1998. DOI: 10.2514/6.1998-438. URL: https://doi.org/10.2514/6.1998-438.

[60] *Boeing 747-100.* URL: http://www.fliegerweb.com/de/lexicon/Airliner/Boeing+747-100-504.

[61] Schmidt Michael. *Ground-Operational Assessment of Novel Aircraft Cabin Configurations.* URL: https://mediatum.ub.tum.de/doc/1381821/1381821.pdf. (accessed: 30.06.2018).

[62] Schmidt et al. *Contribution of Cabin related and Ground Operation Technologies towards FlightPath 2050.* URL: https://www.dglr.de/publikationen/2013/301299.pdf. (accessed: 30.06.2018).

[63] Hospodka Jakub. *Electric taxiing – Taxibot system.* URL: https://www.researchgate.net/publication/304584474%5C_Electric%5C_taxiing%5C_-%5C_Taxibot%5C_system/fulltext/577e4f7008aed807ae7b003d/304584474%5C_Electric%5C_taxiing%5C_-%5C_Taxibot%5C_system.pdf. (accessed: 30.06.2018).

[64] Israel Aerospace Industries. *Electric taxiing – Taxibot system.* URL: http://docs.wixstatic.com/ugd/865bf2%5C_9eb200929c4a42108ecf23d94e5c1379.pdf. (accessed: 30.06.2018).

[65] Charles Alcock. *TaxiBot Ready To Cut Cost and Carbon Footprint for Taxiing.* URL: https://www.ainonline.com/aviation-news/air-transport/2016-10-10/taxibot-ready-cut-cost-and-carbon-footprint-taxiing. (accessed: 30.06.2018).

[66] Aircraft Commerce. *Solutions for improving ground operations efficiency.* URL: https://www.inform-software.com/fileadmin/user%5C_upload/Files/Informationsmaterial/Aviation/112%5C_FLTOPS.PDF. (accessed: 30.06.2018).

[67] Israel Aerospace Industries. *TaxiBot System.* URL: http://www.iai.co.il/Shared/UserControls/Print/PopUp.aspx?lang=en%5C&docid=45171. (accessed: 30.06.2018).

[68] Egbert Torenbeek. *Advanced Aircraft Design: Conceptual Design, Analysis and Optimization of Subsonic Civil Airplanes.* Wiley, 2013. ISBN: 1118568117. URL: https://www.researchgate.net/profile/Vitalii_Pertsevyi/post/Which%5C_have%5C_been_popular%5C_research%5C_topics%5C_in_Aircraft%5C_Design%5C_with%5C_special%5C_reference%5C_to%5C_aerodynamics%5C_in%5C_the%5C_current%5C_times/attachment/59d632e479197b807799093b/AS%5C%3A372221806694400%5C%401465756002502/download/Egbert+Torenbeek-Advanced+Aircraft+Design%5C_+Conceptual+Design%5C%2C+Technology+and+Optimization+of+Subsonic+Civil+Airplanes.pdf.

[69] *SAFETY IN STORAGE,HANDLING AND DISTRIBUTION OF LIQUID HYDROGEN.* 2002. URL: https://h2tools.org/sites/default/files/bp-docs/Doc6%5C_02SafetyLiquidHydrogen.pdf.

[70] mit.edu. *First Law of Thermodynamics.* URL: http://web.mit.edu/16.unified/www/FALL/thermodynamics/notes/node15.html. (accessed: 01.07.2018).

[71] Swedish Standards Institution. *SS-ISO 6976: Natrual gas- Calculation of calorific values, densit, relative density and Wobbe index from composition.* Swedish Standards Institution, 1996.

[72] *European Aviation Environmental Report 2016.* 2016. DOI: 10.2822/385503. URL: https://ec.europa.eu/transport/sites/transport/files/european-aviation-environmental-report-2016-72dpi.pdf.

[73] KOLJA SEECKT. *Conceptual Design and Investigation of Hydrogen-Fueled Regional Freighter Aircraft*. 2010. URL: http://www.fzt.haw-hamburg.de/pers/Scholz/GF/SEECKT-LIC-KTH%5C_DesignHydrogenFueledFreighterAircraft%5C_10-10-25.pdf.

[74] *GREENHOUSE GASES AND GLOBAL WARMING POTENTIAL VALUES*. Apr. 2002. URL: http://steadystaterevolution.org/files/pdf/ghg%5C_gwp.pdf.

[75] EASA.IM.A.196. *TYPE-CERTIFICATE DATA SHEET FOR NOISE*. URL: https://www.easa.europa.eu/sites/default/files/dfu/TCDSN%5C%20EASA.IM%5C_.A.196%5C%20Issue17.pdf. (accessed: 01.07.2018).

[76] Graham Warwick. *Hear This - The BWB is Quiet!* URL: http://aviationweek.com/blog/hear-bwb-quiet. (accessed: 28.06.2018).

[77] J. Thorbeck. *DOC-Assessment Method*. URL: http://www.fzt.haw-hamburg.de/pers/Scholz/Aero/TU-Berlin%5C_DOC-Method%5C_with%5C_remarks%5C_13-09-19.pdf. (accessed: 28.06.2018).

[78] R.W Bohannon. "Comfortable and maximum walking speed of adults aged 20-79 years: reference values and determinants". In: (1997), pp. 16–17.

[79] Y.Li et. al. Y.Liu W.Wang. "A new simulation model for assessing aircraft emergency evacuation considering passenger physical characteristics". In: (2014), p. 191.

[80] *ONE DIMENSIONAL STEADY STATE HEAT CONDUCTION*. URL: http://nptel.ac.in/courses/Webcourse-contents/IISc-BANG/Heat%5C%20and%5C%20Mass%5C%20Transfer/pdf/M2/Student%5C_Slides%5C_M2.pdf.

[81] Loos Eric S. Violette John A. *Mechanical Design of a Variable Pitch Fan for Turbofan Engines*. June 2010.

[82] Casey L. Burley Russell H. Thomas and Erik D. Olson. *Hybrid Wing Body Aircraft System Noise Assessment With Propulsion Airframe Aeroacoustic Experiments*. URL: https://ntrs.nasa.gov/archive/nasa/casi.ntrs.nasa.gov/20100023399.pdf. (accessed: 28.06.2018).

[83] *Airport Infrastructure*. URL: http://de.total.com/de/die-total-gruppe-deutschland/projekte-fuer-bessere-energie-deutschland/die-total-multi-energie-tankstelle-am-ber-berlin-schoenefeld. (accessed: 30.06.2018).